Our responses to the Reviewers are organized as: Reviewer comment in italic and response in blue regular font. The changes made in the manuscript refer to the new version (Page, Line), in bold. References are listed in the end of this section.

After the Reviewer comments and author responses the updated manuscript is appended, with changes marked in red.

## REVIEWER 1:

*This paper presents a two-year monthly time series of measurements of aerosol chemistry (organic and inorganic) from a sampling site in the Ugandan mountains, and area sensitively placed to record seasonal variations in aerosol sources in sub-Saharan Africa. The measurements include radiocarbon and stable carbon isotope determinations on a subset of samples from across the wet and dry seasonal cycle. These measurements enable the delineation of major changes in aerosol source related mostly to a changing input of aerosols derived from savanna burning. While there is nothing that is particularly novel in the results compared to the range of previous work in the region over the last decades, the results do contribute to a growing and useful body of aerosol data from this very large region of the world. The study has been well conducted and a series of robust results generated that clearly show the seasonal impact of savanna burning on local aerosol composition. The source apportionment using carbon isotopes is particularly valuable. I do not have any substantive issues with the analysis or interpretation.*

We thank Reviewer 1 for the overall supportive comments and constructive feedback. We have updated the manuscript accordingly (see details below) and believe that the manuscript is significantly improved.

In response to Reviewers 3 and 4 we have made one larger change in the paper: we have implemented an expanded Bayesian MCMC technique, in which the isotope correlations with TC are used to constrain the sources. This method is based on our work from Martens et al. (2019) – see elaborations in response to Reviewer 4. The method is described in the updated Section 2.5 and the results are discussed in the updated Section 3.5. In connection to this, we have also discussed three sensitivity scenarios, w.r.t, $C_4$ and fossil $\delta^{13}C$ endmembers.

New/changed figures and tables:

**Figure 1:** We have updated Figure 1, now with back-trajectory arrival heights at 100 m.a.g.l., and 500 m.a.g.l. as a new Figure S1. In the submitted version the arrival heights were (by mistake) 10 m.a.g.l, and the latitude was slightly offset. We think 100 and 500 are more representative, while they also in good agreement.

**Figure 4:** We moved the $\Delta^{14}C$ vs TC plot to a new **Figure 5,** in which we also added a $\delta^{13}C$ vs TC plot.

The previous **Figure 5** (2D isotope plot) is the new **Figure 6**.

We have updated the previous **Figure 6** with the results from the new MCMC approach, and this is the new **Figure 7**.

**New Figure S1**: back trajectories at arrival height 500 m.a.g.l.

**New Figure S2:** $\Delta^{14}C$ vs TC and $\delta^{13}C$ vs TC from the new Bayesian MCMC source apportionment method,

**New Figure S3**: A sensitivity analysis of the new Bayesian MCMC source apportionment strategy w.r.t. number of data points.

**New Figures S4-S6:** computed fractional source contributions from 3 alternative endmember scenarios; sensitivity tests.

**New Table S2** with updated fractional source contributions from the new MCMC approach.

**New Tables, S3-S5:** results from the MCMC-based source apportionment from the 3 alternative endmember scenarios.

Reviewer comment: *The paper is possibly somewhat long for the amount of data it presents, and does make some slightly overblown claims about the importance of the results in the context of regional environmental sustainability, climate and health that could be reduced in scope.*

We agree, that the implications may have been over-stated, while we still maintain that the health- and climate impact serves as an important motivation for the study, even though these are not directly addressed. We have removed related parts in the Abstract, the introduction and in the Outlook.

We have updated the manuscript accordingly, including the specific comments by reviewer and the other reviewers, as well as the specific points raised in the annotated supplement to these comments, see below.

*I have also identified a large number of grammatical issues on the attached pdf Please also note the supplement to this comment: https://www.atmos-chem-phys-discuss.net/acp-2019-1027/acp-2019-1027-RC1- supplement.pdf Interactive comment on Atmos. Chem. Phys. Discuss., https://doi.org/10.5194/a*

**Responses to specific comments**

We here respond to specific questions or more substantial changes.

*Page 1, line 22.*

*'major uncertainties of the, e.g., climate and health impacts'*

We change this to:

'In this paper we use ground-based observations to address the currently large uncertainties in source-resolved emission estimation of carbonaceous aerosols.'

**Page 2, Lines 21-23.**

*Page 5, line 117.*

Yes, 1M HCl.

*Page 6, line 130.*

*'The accuracy of the measurement ranges from 7% for 1 mg·$L^{-1}$ of carbon solution to 3% for concentrations higher than 2 mg·$L^{-1}$ of carbon.'*

We have clarified this as:

'The accuracy of the measurement ranges from 7% (70 μg $L^{-1}$) for 1 mg $L^{-1}$ of carbon solution to 3% for concentrations higher than 2 mg $L^{-1}$ of carbon (corresponding to 60 μg $L^{-1}$).'

**Page 6, Lines 138-140**

*Page 8, lines 190-197.*

*'The meteorology of Rwanda is governed by the East African monsoon, with peak rainfalls in in April and November. There are thus two dry seasons, December-January-February (DJF) and the main dry season June-July-August (JAA). The dry periods in SSA are characterized by extensive biomass burning. During DJF the fires mainly occur to the north of Rwanda, and during JJA to the south (Fig. 1). Savannas are the main biomes in SSA, covering ~ 65% of the landmass, and are the main source of fire emissions (Cahoon et al., 1992). Located in a highly elevated region, Rwanda is, broadly speaking, surrounded by savanna regions, except to the west, where the tropical rainforests of Africa are located.'*

We moved this section to the M&M section 2.1 describing the station.

**Page 5, Lines 96 to 103.**

*Page 9, line 214.*

We have changed 'aerosol regime' to 'aerosol sources and atmospheric processing'

**Page 10, Line 241-242**

*Page 10, line 242.*

The OC/EC-ratio is unitless.

*Page 11, line 271.*

TC is defined in the limit $0 \leq TC < \infty$, and is not expressed in units of percentage.

**REVIEWER 2:**

*It's a nice little study that adds to the much-needed set of measurement data in SSA. Novel in the sense data in SSA are missing, but otherwise a mainly normal study. Ambient aerosols have been collected at a remote site in Rwanda and analyzed for their content of carbonaceous species and some ions. The regional influence of savannah fires is nicely confirmed by the isotope measurements. Apart from a few clarifications I would like the authors to do in the manuscript, the analysis and discussion part of the manuscript is OKI, but the claims of impacts on climate and health are outside the focus of the paper. Just as reviewer #1 points out, there are some grammatical mistakes that needs the C1 attention of the authors. I will not repeat the things #1 already mention but add to the list below.*

We thank Reviewer 2 for the overall supportive and constructive comments and suggestions. We have incorporated the majority of the suggestions (see below) and think the paper is now is significantly improved.

In response to Reviewers 3 and 4 we have made one larger change in the paper: we have implemented an expanded Bayesian MCMC technique, in which the isotope correlations with TC are used to constrain the sources. This method is based on our work from Martens et al. (2019) – see elaborations in response to Reviewer 4. The method is described in the updated Section 2.5 and the results are discussed in the updated Section 3.5. In connection to this, we have also discussed three sensitivity scenarios, w.r.t, $C_4$ and fossil $\delta^{13}C$ endmembers.

New/changed figures and tables:

**Figure 1:** We have updated Figure 1, now with back-trajectory arrival heights at 100 m.a.g.l., and 500 m.a.g.l. as a new Figure S1. In the submitted version the arrival heights were (by mistake) 10 m.a.g.l, and the latitude was slightly offset. We think 100 and 500 are more representative, while they also in good agreement.

**Figure 4:** We moved the $\Delta^{14}C$ vs TC plot to a new **Figure 5,** in which we also added a $\delta^{13}C$ vs TC plot.

The previous **Figure 5** (2D isotope plot) is the new **Figure 6**.

We have updated the previous **Figure 6** with the results from the new MCMC approach, and this is the new **Figure 7**.

**New Figure S1**: back trajectories at arrival height 500 m.a.g.l.

**New Figure S2:** $\Delta^{14}C$ vs TC and $\delta^{13}C$ vs TC from the new Bayesian MCMC source apportionment method,

**New Figure S3**: A sensitivity analysis of the new Bayesian MCMC source apportionment strategy w.r.t. number of data points.

**New Figures S4-S6:** computed fractional source contributions from 3 alternative endmember scenarios; sensitivity tests.

**New Table S2** with updated fractional source contributions from the new MCMC approach.

**New Tables, S3-S5:** results from the MCMC-based source apportionment from the 3 alternative endmember scenarios.

*Line 22: While possible fixing the comment from #1, please see to that the final sentence is possible to understand. The current is not.*

This sentence now reads.

'In this paper we use ground-based observations to address the currently large uncertainties in source-resolved emission estimation of carbonaceous aerosols.'

**Page 2, Lines 21-22.**

*L 33: Remove ", an SSA background site"*

Done, thanks.

*L 57-58: Could this be expanded a bit? What is and why is it distinct?*

We have replaced this sentence with

'Ground- and airborne chemical characterization from this and other campaigns suggest a rather distinct aerosol chemical composition, including elevated BC, $K^+$ and $NO_3^-$ concentrations (Table 1).'

**PAGE 3, LINE 54-56.**

*L 68. I miss a climate related reference for the claim. If climate should still be part of the paper.*

We believe that climate is an important motivator for investigating source dynamics of aerosols in SSA.

We added the reference IPCC, 2013.

**Page 4, Line 66**

*L 71-72: I miss a reference for the claim.*

We added the reference to Liousse et al., 2015.

**Page 4, Line 70.**

*L 99 + 102: If only nighttime measurements were done, how can this help a strategy to study diurnal variation? And is that a strategy of this study?*

Diurnal variability was not an aim of this study. We collected 7 days samples, but the sampler was only on during the night.

We now write:

'Night-time only (1AM to 6AM) was conducted to minimize the effects of local emissions and day-time local atmospheric chemistry and to increase likelihood to capture the regional, free troposphere, signals. This strategy is supported by high temporal resolution investigations of the diurnal cycle of, e.g., BC (DeWitt et al., 2019). Each sample was collected over a period of 7 days.'

**Page 5 Lines 107-111**

*L 150: Location of the institute?*

We added location as:

"National Ocean Sciences Accelerator Mass Spectrometry (NOSAMS) facility at the Woods Hole Oceanographic Institute (Falmouth, Massachusetts, USA)"

**Page 7. Line 158**

*L 155-158: If the intention is to show the reader how Fbio is calculated, why not rearrange Eq. 1 into Fbio = . . ..?*

Yes, the Equation now reads:

$$f_{bio} = \frac{\Delta^{14}C_{sample} - \Delta^{14}C_{fossil}}{\Delta^{14}C_{bio} - \Delta^{14}C_{fossil}}$$

*L 167: I think a "=" before +57 would make "Cbio +57 ± 52 ‰'' more readable.*

We agree. We have updated accordingly.

**Page 7 Line 175**

*Section 2.5: The heading and the text are presenting the content in different order. Why?*

We agree this is inconsistent and switched the order.

**Page 9 Line 215**

*Throughout the manuscript: Don't mix "season" and "period". Stick to "season". Change "emissions sources" to "emission sources". "Emissions" appears in other combinations as well, where I think the plural "s" should be removed.*

We agree and have updated accordingl throughout the manuscript.

*L 205: BT not defined. Could be written in full.*

We agree and now write 'back-trajectories' throughout the paper.

*L 220: I normally avoid "as well as other factors" as it is not very helpful for the reader. I think most readers of a aerosol paper understands that we are not in full control of everything in ambient measurements and thus this addition is not needed.*

We agree and removed this part.

*L 222-223: remove one set of "has also". I also miss a reference for this claim.*

Removed. We added Gao et al. (2003) and Formenti et al. (2003), from Table 1, as references.

**Page 10, Lines 250-251.**

*L 237: What activity? Vulcanic? Human?*

Yes, it was unclear and now reads:

'but with no clear linkage to an increase in volcanic $SO_2$ emissions.'

**Page 11, Line 264.**

*L 242: Fig. 3 shows EC/TC, not OC/EC ratio.*

Yes, we choose to plot EC/TC for parallel construction in Figure 3. However, OC/EC is more commonly discussed. We have changed the text as:

'Here, the EC/TC shows a distinct seasonality (Fig. 3 and Table S1). More commonly analyzed, though, is the OC/EC ratio (=(TC-EC)/EC), with elevated levels during the wet season (11±3) compared to the dry season (7±3; Table S1).'

**Page 11 Lines 268-270**

*L 247: Have you considered that there is more plants material that can contribute to the OC in wet season? Can windblown dust during dry season increase the EC concentrations and thus the TC?*

We removed the sentence "The elevated wet-season OC/EC may indicate increased relative influence of local SOA formation." As we think it is too speculative.

*L 248: Is SO2 really elevated during wet season? It looks more random. Volcanic influence?*

The $SO_4^{2-}$/TC levels are more scattered than some of the other ratios, but overall it is higher during the wet seasons (0.29) compared to the dry season (0.22). It is not unlikely that this reflects regional volcanic activity.

We added:

"… including potential volcanic input of $SO_2$"

**Page 11 Line 278**

*L 265: Occasionally? Within your analysis errors they are all above +20.*

We agree and removed 'occasionally'.

*L 277: 12C?*

Good point. We now write:

'An overall enrichment in $^{13}C$ has been found in aged air masses in South Asia, especially for WSOC'

**Page 12 Lines 310-311**

*L 295-298: To me the numbering of the points looks strange. (1.) etc. I would prefer it written in text instead.*

We removed the numbering and now write:

'First, the $\delta^{13}$C-value is not an exclusive source marker, but is also affected by atmospheric processing (e.g., photo-chemical oxidation and secondary formation). Second, the main source categories must be defined and distinguishable using carbon isotopes. Third, the source-values of the isotope-signatures, the endmembers, and their natural variability need to be established.'

**Page 13 Line 327-331**

*L 356-357: Reference to Supplement Table S1? If it is the results in this study that is referred to.*

We agree and added reference to Table S1.

*L 360: Remove one "that"*

Thanks. Done!

*L 365: Why is the site suddenly called a mountain background site? Why not use the name again?*

We agree, and replaced with RCO.

*L 389: "expected rapid change". Is that something that is already happening? If so, can references from 1990's be used for comparisons in the paper? Like "g" in Table 1.*

We agree, in principle: The rapid change is seen in many sectors, including emission inventory estimates (Liousse, 2015). However, given the few ground-based data it is hard to evaluate such trend from observational data; especially when measured at different sites, and campaign-wise.

*Figure 1, and text. The blue lines in the figure comes from the Arabic peninsula. Can you still claim you have no influence of flaring from that region?*

We have updated the back-trajectories with what we think are more realistic arrival heights, 100 and 500 m.a.g.l, compared to 10 m.a.g.l. This suggests a slower influence from the Arabic peninsula.

**New Figures 1 and S1.**

We now write:

'However, given the distances to the RCO station and the prevailing wind directions, emissions from flaring are not expected to affect the site, while the $\delta^{13}$C-signatures for gas-flaring are

strongly depleted in $^{13}C$ ($\delta^{13}C$<-38‰; Winiger et al., 2017) and even a small contribution would shift the observed values significantly.'

**Page 14 Lines 252-355.**

*Figures 2, 3, 5, 6: "The November 2014 to April 2015 gap is due to a lightning strike" only makes a reader curious. I suggest reformulating it. Like "Instruments were hit by lightning resulting in a data gap November 2014 to April 2015"*

Thanks. We have updated accordingly.

*Figure 3: In the bottom graph there is an extra "+" after TC in the legend.*

Thank you. We have removed the +.

## REVIEWER 3:

*Anonymous Referee #3 Received and published: 20 December 2019 "Seasonal source variability of carbonaceous aerosols at the Rwanda climate Observatory" by Andersson et al. The manuscript reports results of ground-based observations of carbonaceous aerosol at a mountain site in Rwanda, sub-Saharan Africa. Fine airborne particulate matter (PM2.5) was collected weekly basis on quartz fibre filters, then total carbon, organic carbon, elemental carbon, water-soluble organic carbon contents and their radio and stable isotopes were analyzed. Major inorganic ions (nitrate, sulfate, ammonium, and potassium ions) were also analyzed. Mass balance approach was applied to the isotopic data to identify the origins of the carbonaceous aerosols. The results were also compared with wild fire information provided by NASA and with back trajectories of air masses arriving at the sampling site using HYSPLIT provided by NOAA to better understand the origins. Studies of origins of airborne particulate organic matter are one of the hottest themes in atmospheric science, but the origins are complex and not easy to be untangled. Application of isotopes measurements will provide additional dimension in the scientific information, thus, ideal for such studies. I have been aware of the authors' previous work, the dual isotope analysis, and the analysis provides insight into the origins of organic carbons, particularly differentiation between biogenic and fossil fuel origins using 14C. Compared to 14C, the method of 13C fingerprinting is week due to its large variation of the end members, depending on source types. Here, the authors attempted estimation of carbonaceous aerosols derived from C3 and C4 plants, which are known to have discrete compositions in 13C from each other. Papers reporting those fingerprints of organic aerosols are not many (Mkoma et al., 2014, TellusB; Irei et al., EST, 2014). The 13C fingerprinting approach to the carbonaceous aerosols that contain secondary organic aerosols would not be as simple as the authors describe here, but the studied location may be close enough to capture primary carbons. As I read this manuscript, the analysis was relatively straightforward, and gained results sound reasonable.*

We thank Reviewer 3 for this overall positive assessment of our work, and for constructive feedback, based on which we think the manuscript is significantly improved.

New/changed figures and tables:

**Figure 1:** We have updated Figure 1, now with back-trajectory arrival heights at 100 m.a.g.l., and 500 m.a.g.l. as a new Figure S1. In the submitted version the arrival heights were (by mistake) 10 m.a.g.l, and the latitude was slightly offset. We think 100 and 500 are more representative, while they also in good agreement.

**Figure 4:** We moved the $\Delta^{14}C$ vs TC plot to a new **Figure 5,** in which we also added a $\delta^{13}C$ vs TC plot.

The previous **Figure 5** (2D isotope plot) is the new **Figure 6**.

We have updated the previous **Figure 6** with the results from the new MCMC approach, and this is the new **Figure 7**.

**New Figure S1**: back trajectories at arrival height 500 m.a.g.l.

**New Figure S2:** $\Delta^{14}C$ vs TC and $\delta^{13}C$ vs TC from the new Bayesian MCMC source apportionment method,

**New Figure S3**: A sensitivity analysis of the new Bayesian MCMC source apportionment strategy w.r.t. number of data points.

**New Figures S4-S6:** computed fractional source contributions from 3 alternative endmember scenarios; sensitivity tests.

**New Table S2** with updated fractional source contributions from the new MCMC approach.

**New Tables, S3-S5:** results from the MCMC-based source apportionment from the 3 alternative endmember scenarios.

*However, I also had impression that they could go into a fairer evaluation that considers the possible variation in the 13C compositions of endmembers. For example, according to L177-179, they performed Monte Carlo simulation to estimate the uncertainties of fC3, fC4, and ffossil propagated from the variability of fingerprinting 13C compositions. The gained uncertainties were small enough to capture significant values of source contributions and then plotted in Figure 6. At the same time Figure 5 shows wide ranges of the 13C compositions for the end members, C3, C4 plants and fossil fuel. Are those variations reflected to the uncertainties of the source apportionment? Such large variations do not seem to end with the uncertainties in Figure 6. If not, I recommend the authors to work on more objective evaluation by providing a several scenarios with the combinations of different 13C compositions of the three endmembers, together with the most feasible apportions (probably those currently described in the manuscript). This will raise the quality of this manuscript, I believe.*

We agree with the over-arching comments on the treatment of the endmember variability, and in response to both reviewer 3 and reviewer 4 we now implement a more advanced Bayesian MCMC methodology and explore different endmember scenarios. We have updated sections 2.5 and 3.5 accordingly.

New description of the MCMC technique in M&M Section 2.5:

‘The vegetation in SSA may be divided into two main photosynthetic classes: $C_3$-plants and $C_4$-plants, see discussion in Section 3.5. These two groups have distinct $\delta^{13}C$-signatures, allowing isotope-based separation. We may then resolve three source classes by combining $\Delta^{14}C$ and $\delta^{13}C$: $C_3$-plants, $C_4$- plants and fossil, through isotopic mass-balance (Andersson et al., 2015):

$$\begin{pmatrix} \Delta^{14}C(i) \\ \delta^{13}C(i) \\ 1 \end{pmatrix} = \begin{pmatrix} \Delta^{14}C_{C3} & \Delta^{14}C_{fossil} & \Delta^{14}C_{C4} \\ \delta^{13}C_{C3} & \delta^{13}C_{fossil} & \delta^{13}C_{C4} \\ 1 & 1 & 1 \end{pmatrix} \begin{pmatrix} f_{C3}(i) \\ f_{fossil}(i) \\ f_{C4}(i) \end{pmatrix} \quad (2)$$

Endmember variability may significantly influence the calculated source fractional contributions (Andersson, 2011). For a discussion on the specific endmember ranges used here, see Section 3.5.

In Eq. (2) the isotopic data is treated as independent. However, here we find that there is a dependence between the isotope ratios and the TC concentrations, such that $\Delta^{14}C(i) \sim A/TC(i) + B$, where A and B are constants, and i is the sample index (Fig. 5). This is known as a Keeling relation, and is discussed in more detail in Section 3.4. The relation holds for both $\Delta^{14}C$ ($R^2$=0.85, $p<0.01$) and $\delta^{13}C$, while the correlation is weaker for $\delta^{13}C$ ($R^2$=0.55, $p<0.1$). A method for using correlations within the framework Bayesian source apportionment has recently been developed (Martens et al., 2019). The rationale is based on both statistical concepts and the averaging expected from atmospheric mixing. The endmember ranges used in the calculations are from isolated sources, but during long-range transport the variability within a given source, e.g., savanna fires, will be reduced. Using correlations between data points, a means for accounting for the mixing is obtained, and more realistic source fraction estimates are obtained. When using the estimated source fractions to back-calculate the isotope signatures, the agreement is good compared with direct fits (Fig. 5 and Fig. S2). A sensitivity analysis is discussed in section 3.5 (Fig. S3)

To account for the correlations in the data-set we therefore add a second constraint in the source apportionment calculations, based on the relation to the TC concentrations:

$$\begin{pmatrix} f_{C3}(i) \\ f_{fossil}(i) \\ f_{C4}(i) \end{pmatrix} = \frac{1}{[TC(i)]} \cdot \begin{pmatrix} f_{C3,slope} \\ f_{fossil,slope} \\ f_{C4,slope} \end{pmatrix} + \begin{pmatrix} f_{C3,intercept} \\ f_{fossil,intercept} \\ f_{C4,intercept} \end{pmatrix} \quad (3)$$

Where we, instead of fitting a source vector ($f_{C3}$, $f_{fossil}$, $f_{C4}$) for each individual data pair, fit two vectors: a slope and an intercept of the line, to all data points. This clearly holds the advantage of have fewer fitting parameters. We emphasize that the strength of the correlation of the isotope signatures relative to 1/TC is naturally incorporated into this relation, such that lower correlation of $\delta^{13}C$ w.r.t 1/TC impose weaker constraints on the calculated source fractions, compared to $\Delta^{14}C$.'

**Pages 8-9, Lines 178-206.**

New text on the sensitivity of the new MCMC approach w.r.t. number of data points in R&D Section 3.5:

'Back-calculating the isotope signatures from the computed source fractions from the MCMC-simulations essentially reproduce the Keeling relations relative to 1/TC (Figs. 5 and S2). To check influence of the number of data points used in the Keeling-based MCMC, we computed comparative scenarios where every third data point was used (starting at data point 1, 2 and 3 respectively) (Fig S3). The standard deviations for the calculated $f_{C3}$ are on average doubled when only every third point are used (5% vs 10%), showing how correlations between multiple data points aids in constraining the sources.'

**Page 15 Lines 388-394**

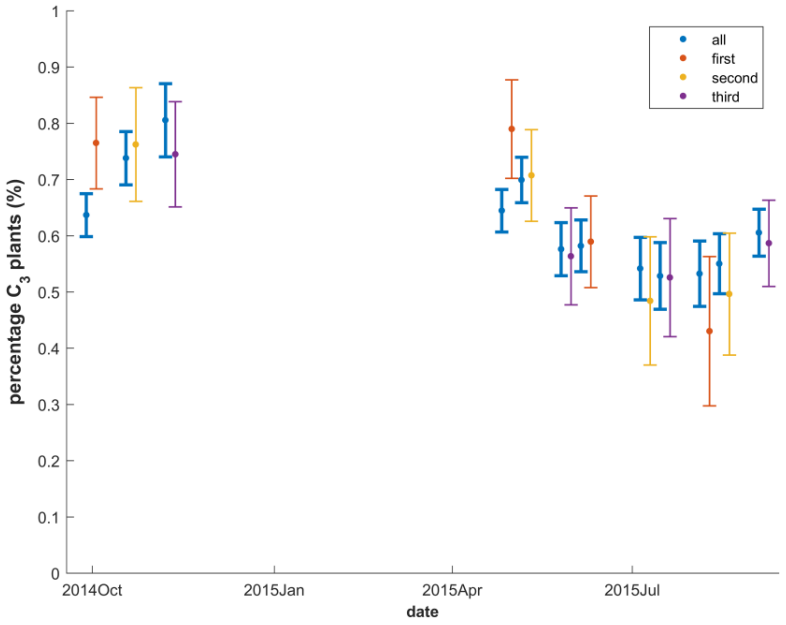


**NEW Figure S3** Sensitivity of the Keeling-based Bayesian MCMC source apportionment approach w.r.t. number of data points in the calculation. The fraction $C_3$-plants is plotted vs time. In blue, the results from using all 12 data pairs (errorbars: mean ± stdev). The orange, yellow and purple lines show calculations using every third data point, starting from data point 1, 2 and 3, respectively. The results from every third data points are shifted slightly in time (to the right) for visual clarity.'

Discussion on estimating the influence on KIE on the $C_4$ $\delta^{13}C$ endmember:

'Accounting for such effects in source apportionment is a challenge, especially since the reported values are ranges and not mean and variability, and thus are highly influenced by potential outliers. We here use a method discussed in Andersson et al. (2015) to address the issue of statistical analysis of ranges by assuming that the total range corresponds to the 95% confidence intervals of a normal distribution. This corresponds to the range of 4 times the standard deviation, yielding $\sigma$ = 7/4‰, while the mean is -7/2‰. Combining this with the variability of the of pure $C_4$-plants we obtain: $\delta^{13}C_{C4}$: -16.6 ± 2.2‰, where $\sigma^2 = 1.2^2 + (7/4)^2$ ‰$^2$. These values are also what is obtained by numerical estimation of the convolution of a normal distribution ($\mu$ = -16.6, $\sigma$ = 1.2‰) with a uniform distribution ([-7, 0] ‰), adding to the strength of statistical representation.'

**Pages 14-15 Lines 369-377**

Discussion on endmember sensitivity scenarios:

'Since the $\delta^{13}C$ endmembers for, in particularly $C_4$-plants, are not well-constrained, we also employed a sensitivity analysis w.r.t. endmembers and the potential influence of KIE (Tables S2 – S5 and Figs. S4 – S6). In addition to the above discussed best estimate scenario, we tested two $\delta^{13}C_{C4}$ scenarios: a 'minimum KIE scenario' with zero KIE ($\delta^{13}C_{C4}$ -13.1±1.2‰) and a 'maximum KIE scenario', with a depletion by 5.9‰ ($\delta^{13}C_{C4}$ -19.0±2.2‰). The maximum KIE scenario was established such as the $f_{C4}/(f_{C4}+f_{C3})$-ratio would be 62% as TC approach infinity, and thus 100% savanna contributions, see Eq. (4). As expected, these scenarios significantly shift the estimated relative $C_4$ contributions, resulting in a total range of the sample period averages of 24% (min-KIE; min 6% max 32%) to 42% (max-KIE; min 10%, max 58%), thus providing lower and upper bounds (Figs. S4 and S5 and Tables S3 and S4). The corresponding value for our best estimate is 32% (max 44%, min 8%). In addition, we investigated a scenario with a 3‰ depletion of the fossil endmember ($\delta^{13}C_{fossil}$ -28.5±1.3‰). Since the fossil contribution is overall low as determined by $\Delta^{14}C$, and since $\Delta^{14}C$ constrains the fossil contribution independently of the $\delta^{13}C$ data, this shift has no significant influence on the computed source fractions 6% (max 11%, min 3%) (Fig. S6 and Table S5). Overall, we stress that these three sensitivity test scenarios represent extreme limits, and the a priori least biased scenario is the initially outlined best scenario.'

**Pages 14-15, Lines 395-410.**

**We have also updated related Figures, 5 and 7, and added Figures S3 – S6 and Tables S3 to S5 in the supplementary information, see also Figures below.**

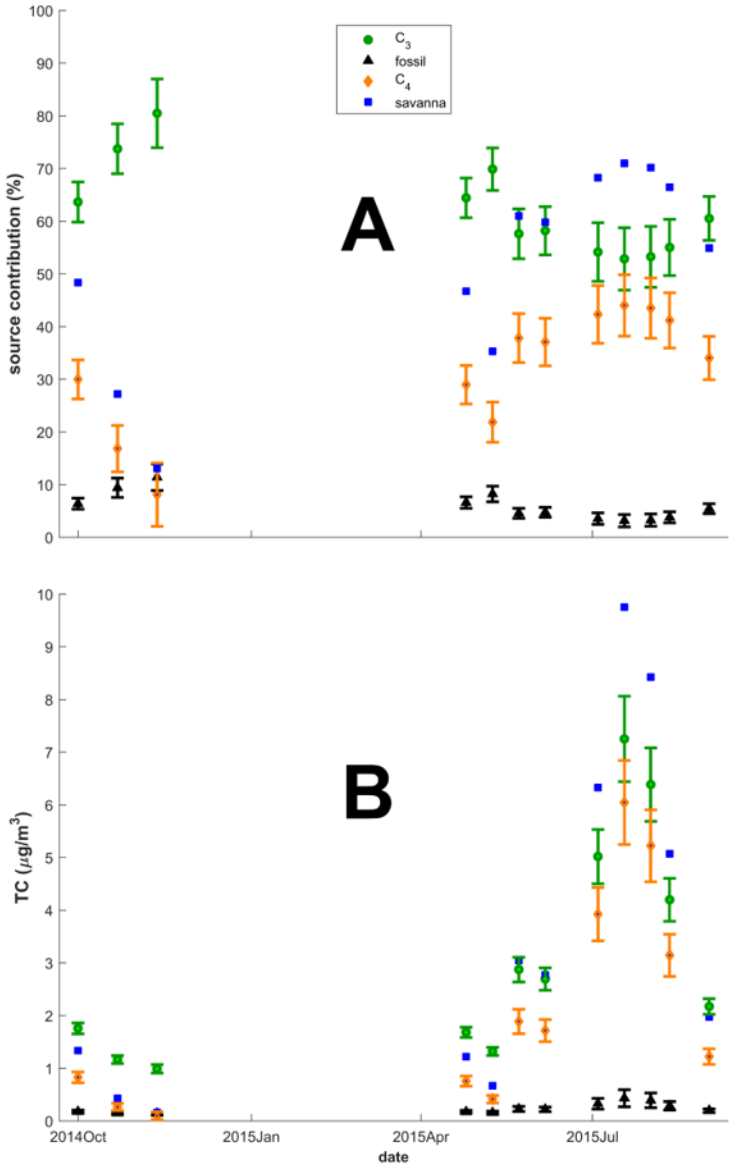


**NEW Figure 7:** Carbon isotope source-segregated fractions and concentrations of TC vs time computed with the 'best endmember scenario'. Panel A. Relative source contributions (%) of $C_3$-plants (green circles), $C_4$-plants (orange diamonds) and fossil (black triangles). Estimated savanna contributions are shown as blue squares. Panel B. Source segregated concentrations of TC of $C_3$-plants (green circles), $C_4$-plants (orange diamonds) and fossil (black triangles). The error bars (standard deviations) were calculated using Markov chain Monte Carlo simulations.

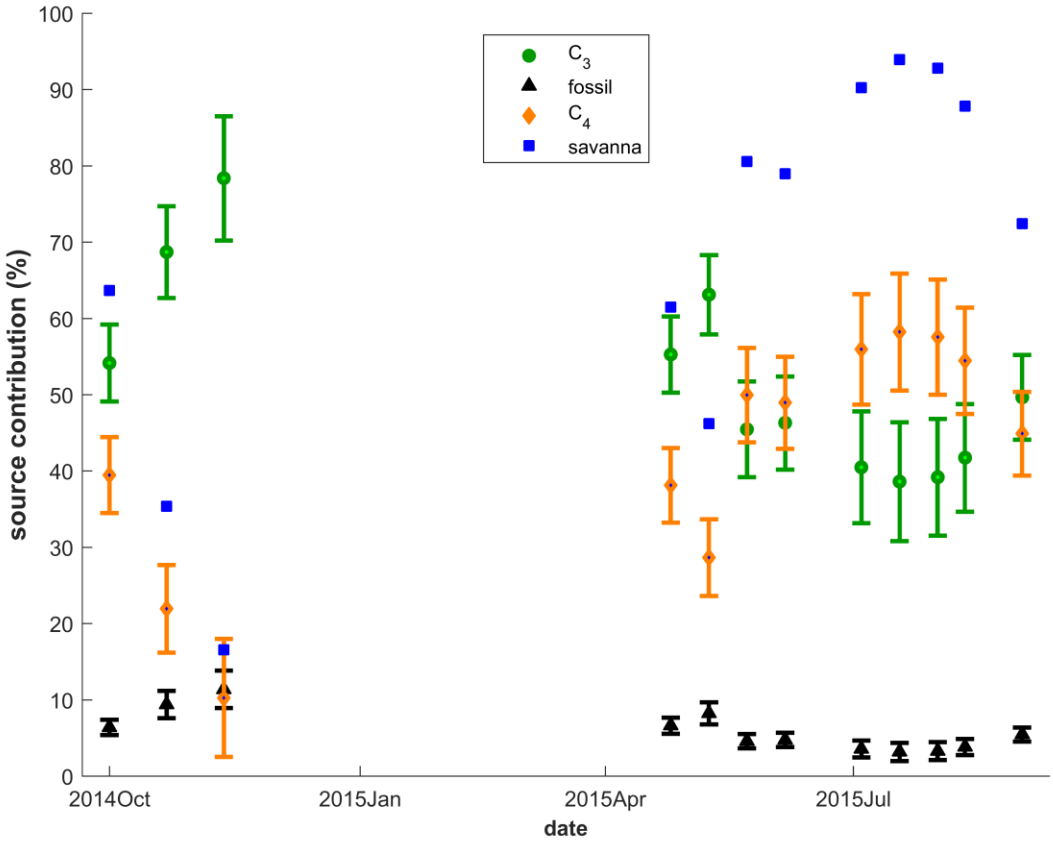


**NEW Figure S4:** Carbon isotope-source segregated fractions and concentrations of TC vs time computed with the 'maximum $C_4$ scenario'. Panel A. Relative source contributions (%) of $C_3$-plants (green circles), $C_4$-plants (orange diamonds) and fossil (black triangles). Estimated savanna contributions shown as blue squares. The error bars (standard deviations) were constrained using Markov chain Monte Carlo simulations. Panel B. Source segregated concentrations of TC of $C_3$-plants (green circles), $C_4$-plants (orange diamonds) and fossil (black triangles).

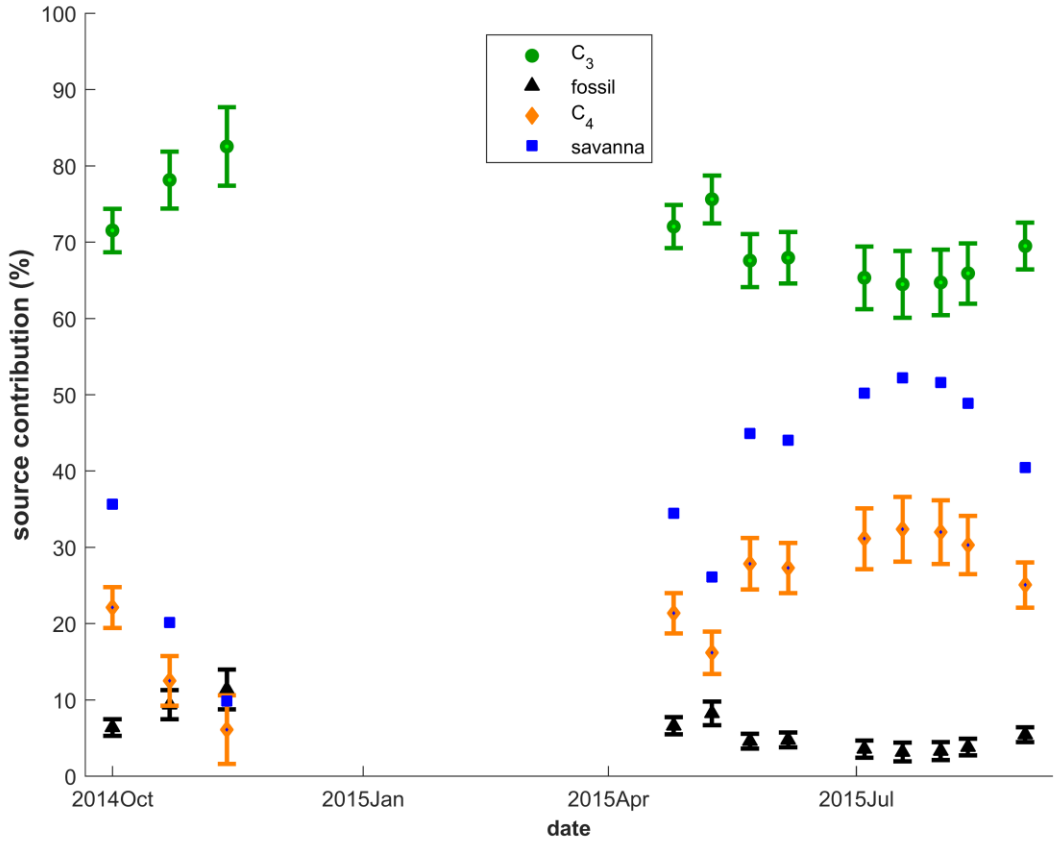


**NEW Figure S5:** Carbon isotope-source segregated fractions and concentrations of TC vs time computed with the 'minimum $C_4$ KIE scenario'. Panel A. Relative source contributions (%) of $C_3$-plants (green circles), $C_4$-plants (orange diamonds) and fossil (black triangles). Estimated savanna contributions shown as blue squares. The error bars (standard deviations) were constrained using Markov chain Monte Carlo simulations. Panel B. Source segregated concentrations of TC of $C_3$-plants (green circles), $C_4$-plants (orange diamonds) and fossil (black triangles).

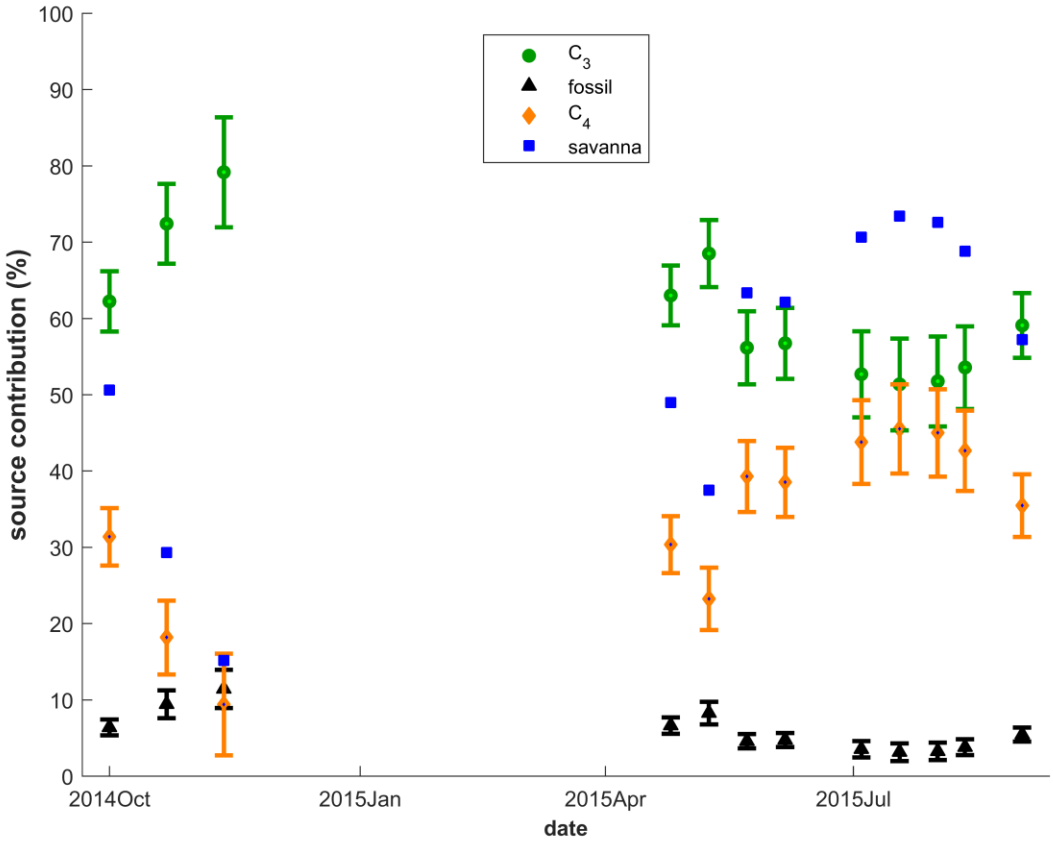


**NEW Figure S6:** Carbon isotope-source segregated fractions and concentrations of TC vs time computed with the 'depleted fossil scenario'. Panel A. Relative source contributions (%) of $C_3$-plants (green circles), $C_4$-plants (orange diamonds) and fossil (black triangles). Estimated savanna contributions shown as blue squares. The error bars (standard deviations) were constrained using Markov chain Monte Carlo simulations. Panel B. Source segregated concentrations of TC of $C_3$-plants (green circles), $C_4$-plants (orange diamonds) and fossil (black triangles).

*My comments on specific parts of the manuscript are provided below.*

*Abstract: Remove "(PM2.5)" because the abbreviation is not repeated in the abstract.*

Yes, removed.

*L98: Add the manufacturer information for PM2.5 inlet. Please provide the information of sampling frequency and duration.*

The manufacturer for the inlet is the same as for the pump. We moved the manufacturer to the end of the sentence, and added 7 days sampling.

**Page 5 Line 107**

*L151-152: Please provide the model and manufacturer information for AMS and IRMS.*

The isotope-ratio measurements were conducted by personnel at the NOSAMS facility. To our knowledge they assembled their own instruments.

https://www.whoi.edu/nosams/ams-instruments

*L192: Correct JAA to JJA. L193-194: Figure 1 does not show distinct plots of wild fires for the JJA and DJF periods. The authors may want to show two plots showing two periods.*

We agree that this would make sense. Unfortunately, DJF was the period when our sampler was broken due to a lightening strike so we do not have any chemical/isotope data for this period, and we therefore remove the reference to the DJF period in Figure 1,

We changed the sentence to:

'During JJA the fires mainly occur to the south of Rwanda (Fig. 1).'

**Page 5, Line 99**

*L205: Please define "BT".*

Thanks. We now spell out 'back trajectories' throughout the manuscript.

*L214-215: "This variability suggests. . ." needs supporting information (i.e., references).*

We disagree on this point. This is an inference.

*L221: Replace "-" with commas.*

We have updated accordingly.

*L223: Provide references directly here instead of "Table 1 that refers references.*

This point was also raised by reviewer 2. As there are 10 references to the Table, we now write:

"However, it is also typically elevated in emissions from savanna fires (Table 1; e.g., Gao et al., 2003; Formenti et al., 2003)."

**Page 10 Lines 250-251**

*L224-226: Please explicitly state whose results have agreed with the observations here.*

We have changed the sentence to read:

"The dry season concentrations of carbonaceous aerosols components and inorganic ions reported here are overall in good agreement with the concentrations observed dry season rural and aged savanna fire air masses (Table 1)."

**Page 10 Lines 252-253**

*L227-230: I am not sure where I can find the evidence showing the decrease and effect. Please describe the location of this information specifically.*

This data is presented in the referenced Table 1, where different stages of plumes are described, e.g., 'fresh', 'aged' etc.

*L241-242: Both Figure 3 and Table S1 do not show OC/EC ratios. Please provide those.*

This point was also brought up by reviewer 2. In figure 3 we wanted to plot EC/TC for parallel construction with all Panels. However, OC/EC is a more commonly used parameter. We now write:

"Here, the EC/TC shows a distinct seasonality (Fig. 3 and Table S1). More commonly analyzed, though, is the OC/EC ratio (=(TC-EC)/EC), with elevated levels during the wet season (11±3) compared to the dry season (7±3; Table S1)."

**Page 11 Line 268-270**

*L246-247: There would be many possible reasons for this variation, and I do not agree with the statement of "The elevated wet-season. . .". I recommend either to remove this sentence or provide the evidence to justify this possibility.*

We agree and removed this sentence.

*L255: I recommend to replace "a pulse" with a different term. How about occasional input?*

We agree and have changed to 'occasional input'

**Page 11 Line 283**

*L271: Avoid symbols of arrow and infinity in the text.*

We agree and now write 'as TC approaches infinity'.

**Page 12 Line 300**

*L277-278: In my opinion, descriptions of "d13C enrichment" and "13C/12C ratio enrichment" are not correct, but enrichment in (or with) 13C is the correct description. Please consider this throughout the text.*

We agree and have updated throughout.

*L275-281: I am not sure the point the authors want to make in this paragraph. Occurrence of chemical reactions in the particle? Please re-write it to make the point clearer.*

Thank you for allowing us to clarify. The point is that $\delta^{13}C$ influenced by KIE, while $\Delta^{14}C$ is not.

We now write:

'In contrast to $\Delta^{14}C$, the $\delta^{13}C$-value is influenced by both atmospheric processes (i.e., kinetic isotope effects, KIE) and source signatures. Here, the $\delta^{13}C$-value shows a similar pattern relative

to the $\Delta^{14}C$-value, depleted in $^{13}C$ (min $\delta^{13}C$ = -27‰) during wet seasons, and higher during the dry season (max $\delta^{13}C$ = -21 ‰) (Fig. 4B). The correlation w.r.t. 1/TC ($R^2$=0.55, p<0.1) is weaker compared to $\Delta^{14}C$ (Fig. 5B). The direct fossil vs biomass source correlation from the $\Delta^{14}C$ Keeling curve is also driving the $\delta^{13}C$-signatures, but the higher variability is explained by larger endmember variability and potential influence of KIE, see Section 3.5. An overall enrichment in $^{13}C$ has been found in aged air masses in South Asia, especially for WSOC (Kirillova et al., 2013; Dasari et al., 2019), but less so for TC. In fact, the enrichment of $^{13}C$ in WSOC often appears to be counter-acted by a decrease in water-insoluble OC (e.g., Yan et al., 2017; Fang et al., 2017).'

**Page 12 Lines 304-313**

*L284: Please provide the degree of "shift" specifically. Also replace "around" with "∼" sign, or vise versa.*

Thank you. We now write:

"However, the temporal trend appears shifted in the RCO samples from values around -25 ‰ to around 22 ‰ in mid-May

**Pages 12-13 Lines 315-317**

*L286: Not sure what agreed in. Please make this specific.*

Thank you for pointing out unclarities. The sentence now reads:

"In addition to the complications of comparing measurements conducted at different sites during different years, there is a good agreement in the $\delta^{13}C$-values, and the temporal offset may be explained by inter-tropical convergence zone position variability.'

**Page 13 Line 317-320**

*L287* Please define "ITCZ".*

We now spell out 'inter-tropical convergence zone', see above comment.

*L303: State Figure 3 when discussion the results shown somewhere.*

We agree. Updated accordingly.

*L330: Replace "between" with from.*

We agree. Updated accordingly.

*L331-334: As I mentioned earlier, I recommend to analyze possible variations in more detail, then provide this fingerprinting d13C that gives feasible results. Choice of this value without other possibilities will lead a biased interpretation.*

We have significantly expanded upon this part in the new version of the manuscript. See response to the over-arching comments by the reviewer.

*L340-342: I am not sure why the authors can say so. Please provide the evidence (observations or references demonstrating such characterizations).*

We think this conclusion is more evident within the new MCMC source apportionment strategy.

See response to the over-arching comments by the reviewer.

*L355-356: Does Figure 6 show 71% of carbonaceous aerosols from savanna fire in the dry season? I do not know where I can find this information in the figure.*

We have updated this section with the results from the new MCMC source apportionment strategy and included the estimated savanna results as blue squares, in the New Figure 7, see above.

*L360-390: I recommend to rewrite "Outlook" because some indirect topics, such as CO2 source and brightening stuff, are referred with many references.*

We agree, and have reduced references and discussion on such topics, while still maintain that parts of the original text is relevant, as this is an outlook section (not a summary or conclusion).

*Table 1: Correct "BC/EC".*

In some of the references the BC was estimated by light-absorption ('BC') but in some as EC.

*Figure 1: As I mentioned earlier, provide two plots for two seasons.*

Please see response to earlier comment.

*Figure 2: The scales of y-axes are overlapped. Please fix those.*

Thank you for noting this. Now fixed.

*Figure 4c: It is interesting to see such a relationship. If extrapolating the curve to zero of TC, which is originated from plant burning, what the intercept value would be? I recommend to briefly discuss this value in the text.*

We definitely see how this could be of interest. However, as TC approach zero, the isotope signature approaches negative infinity; clearly non-physical. The Keeling-relation is based having a variable source and a background. But the background is not zero.

*Figure 5: I recommend to refer the references for d13C of C3, C4, and fossil in the footnote.*

Although we in principle agree, we think reference to Section 3.5 is sufficient, as the list is rather long.

*Figure 6: Add the horizontal line of zero for panel A. By the way, all figure captions should be under the figures. Are those just the style of ACPD?*

Yes, the legends are now located below the figures. We have replaced the previous Figure 6 with a corresponding novel Figure 7, see above.

*Table S1: Refer inorganic components in the table heading as well*

Thank you. Now done.

## REVIEWER 4:

Our responses to the Reviewer are organized as: Reviewer comment in italic and response in blue regular font. The changes made in the manuscript refer to the new version (Page, Line), in bold.

*The study of Andersson et al. reports dual isotope analysis method applied to particulate matter in African Savannah region. The study presents little scientific advancement and the value is only related to relatively scarce data from the region impacted by regional biomass burning. However, even that aspect is somewhat compromised due to observational platform located outside biomass burning region to assess full extent of biomass fires. Most of the connecting trajectories do not overpass fire impacted region and not surprisingly reports relatively low concentrations hardly possessing environmental concern. The site is important remote location for climatic observations, but hardly suitable to assess the impact and extent of regional biomass burning. It is, therefore, important to separate samples collected in fire connecting air masses versus unaffected ones to reveal the extent more convincingly. The applied methods are well suited, but their application and especially discussion needs significant improvement. Dual isotope method is well established, but uncertainties related to C13 are downplayed to suit author's narrative. Given combined contribution to C13 ratio from three competing sources (C3, C4 plants and fossil sources) on top of kinetic fractionation affecting the ultimate ratio, uncertainty analysis needs to be much better elaborated and taken into consideration. Monte Carlo simulation is fine, but there is no information on bench-marking – what was the arbiter for the best solution? How Monte Carlo simulation compared to the observed isotope ratios? The paper can be accepted for publication in ACP, but given little scientific advancement requires much more objective consideration of sources, associated uncertainties and Monte Carlo simulation benchmarking.*

We thank Reviewer 4 for overall positive assessment for carefully scrutinizing the manuscript and providing valuable suggestions for improvements and clarifications.

We agree with Reviewer (and, in fact, all four reviewers) that the main contributions of the present study lie in the addition to the currently scarce data available for Africa and the isotope-based source constraints. The majority of the overall few ground-based data for Africa are from the western and southern parts, while for central SSA (i.e. Rwanda and neighboring countries) the data is even more scarce. We do emphasize that the present study is the first ever to present $^{14}C$-derived source constraints for aerosols at any site in Africa. As such, it is the first to unambiguously differentiate the relative biomass vs fossil fuel contributions with high precision. The strong correlation ($R^2 = 0.85$, $p<0.01$) between the $^{14}C$-signature and the inverse of TC concentrations (the Keeling relation) is not only unusual for aerosols - at least we have not found such relations in our previous studies at receptor sites in the Arctic, or South or East Asia (e.g., Winiger et al., 2017; Fang, et al., 2018; Budhavant et al., 2015) - but also provides a clear interpretation: two components explain the source variability at RCO, a background and a seasonally varying biomass source.

The reviewers' comments made us identify three overarching problems with the submitted manuscript. 1.) The representativity of the station w.r.t., air mass transport, 2.) the description of the Monte Carlo techniques and 3.) the statistical treatment of endmember variability, also raised by reviewer 3. We now believe that we comprehensively have addressed these issues, and that the new version of the manuscript is significantly improved.

New/changed figures and tables:

**Figure 1:** We have updated Figure 1, now with back-trajectory arrival heights at 100 m.a.g.l., and 500 m.a.g.l. as a new Figure S1. In the submitted version the arrival heights were (by mistake) 10 m.a.g.l, and the latitude was slightly offset. We think 100 and 500 are more representative, while they also in good agreement.

**Figure 4:** We moved the $\Delta^{14}C$ vs TC plot to a new **Figure 5,** in which we also added a $\delta^{13}C$ vs TC plot.

The previous **Figure 5** (2D isotope plot) is the new **Figure 6**.

We have updated the previous **Figure 6** with the results from the new MCMC approach, and this is the new **Figure 7**.

**New Figure S1**: back trajectories at arrival height 500 m.a.g.l.

**New Figure S2:** $\Delta^{14}C$ vs TC and $\delta^{13}C$ vs TC from the new Bayesian MCMC source apportionment method,

**New Figure S3**: A sensitivity analysis of the new Bayesian MCMC source apportionment strategy w.r.t. number of data points.

**New Figures S4-S6:** computed fractional source contributions from 3 alternative endmember scenarios; sensitivity tests.

**New Table S2** with updated fractional source contributions from the new MCMC approach.

**New Tables, S3-S5:** results from the MCMC-based source apportionment from the 3 alternative endmember scenarios.

We detail our responses and actions to these main comments below, while responses to the specific comments comes after.

1.) Back-trajectories:

We thank the Reviewer to highlighting concerns regarding the back-trajectories. This made us go back and re-evaluate them. The arrival height, 1600 m.a.s.l., used in the manuscript is 10 m.a.g.l. However, this height is low, and our original intention was to use 100 m.a.g.l.; the discrepancy is explained by an erroneous input of the height of Mt. Mugogo, 1500 compared to the actual 1590. To resolve this issue, we have now re-computed the back-trajectories for two arrival heights: 100 m.a.g.l. (1690 m.a.s.l.) and 500 m.a.g.l. (3090 m.a.g.l), see below response figures R1 and R2:

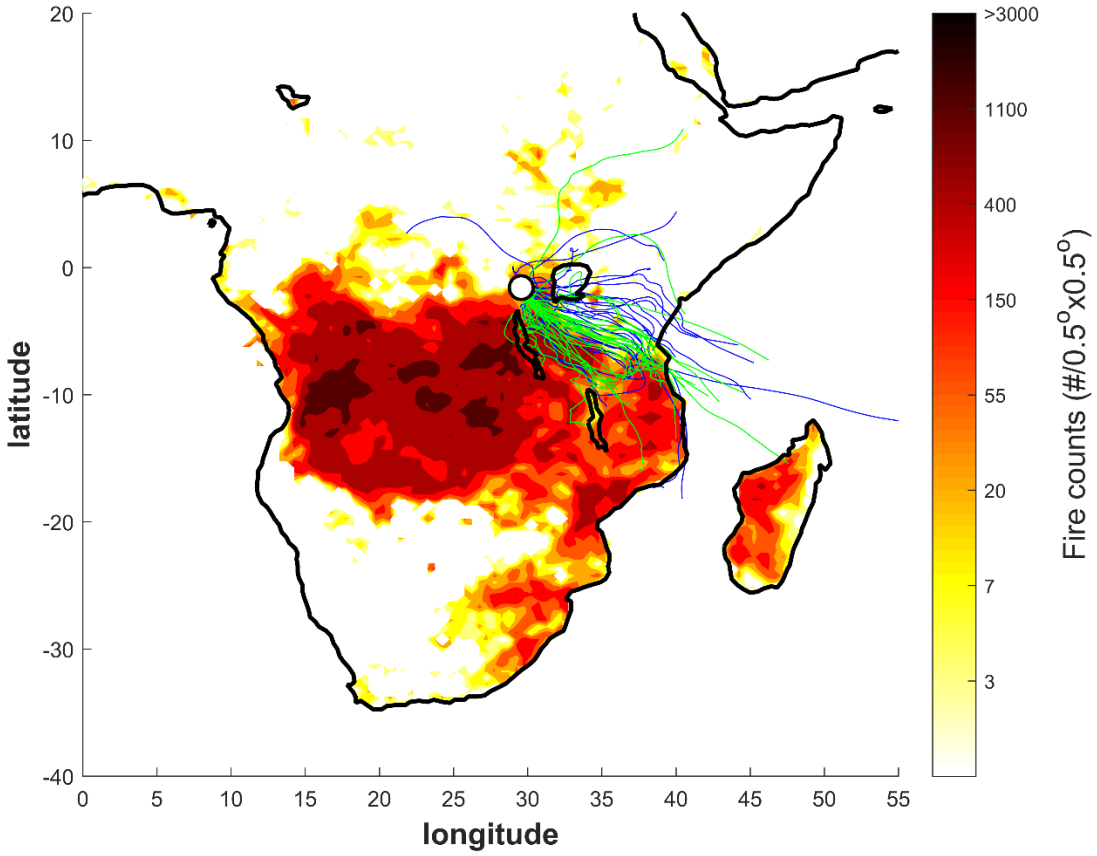


**Figure R1** Fire counts and air mass back trajectories for the October 2014 to September 2015 campaign at the Rwanda Climate Observatory (RCO, black and white circle). The fire counts arefrom the Fire Information for Resource Management System (FIRMS) derived from the NASA 659 Moderate Resolution Imaging Spectroradiometer (MODIS) satellite product for June-July-August (JJA), 2015. The thin lines represent daily (4AM, C.A.T.) 5-day air mass back-trajectories arriving at RCO 100 m.a.g.l. (2690 m.a.s.l.). The blue lines correspond to what we here refer to the 'wet' period (October-November 2014 and April-May 2015), whereas the green lines represent the dry JJA period.

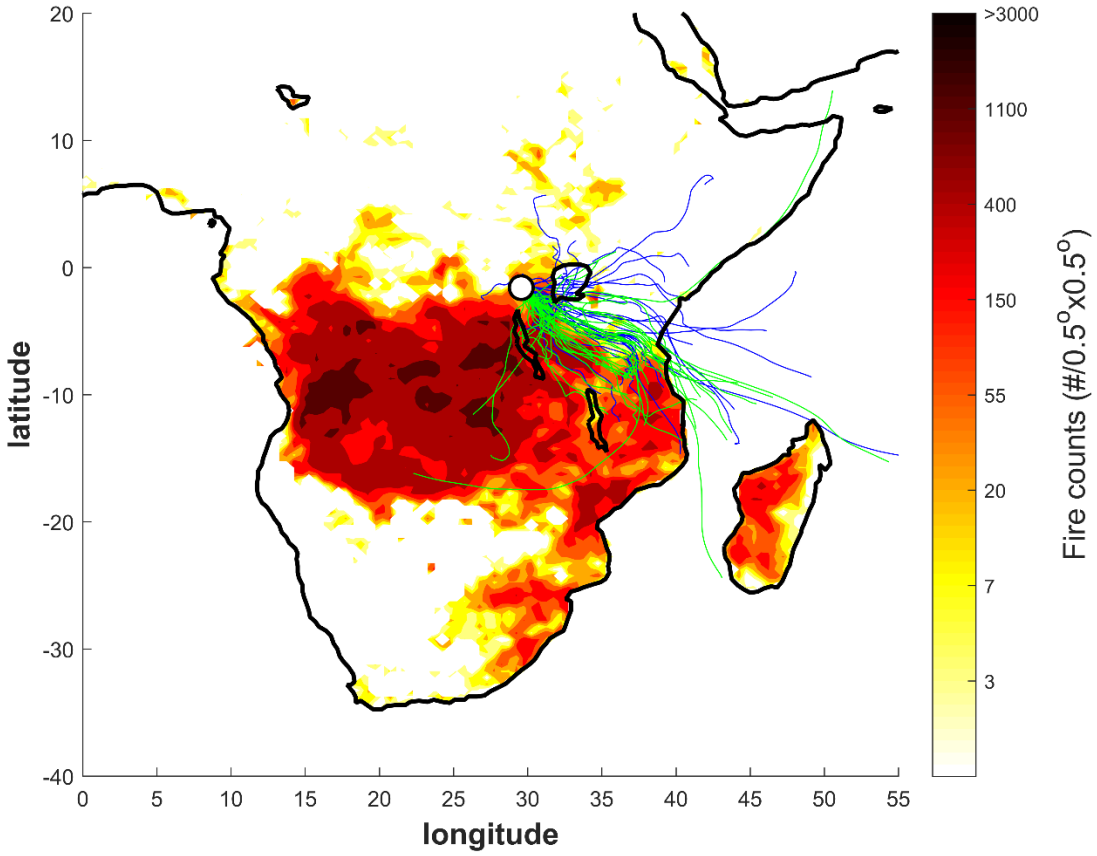


**Figure R2** Fire counts and air mass back trajectories for the October 2014 to September 2015 campaign at the Rwanda Climate Observatory (RCO, black and white circle). The fire counts arefrom the Fire Information for Resource Management System (FIRMS) derived from the NASA 659 Moderate Resolution Imaging Spectroradiometer (MODIS) satellite product for June-July-August (JJA), 2015. The thin lines represent daily (4AM, C.A.T.) 5-day air mass back-trajectories arriving at RCO 500 m.a.g.l. (3090 m.a.s.l.). The blue lines correspond to what we here refer to the 'wet' period (October-November 2014 and April-May 2015), whereas the green lines represent the dry JJA period.

Taken together, we find that the reviewer's comment on the representativity of RCO for capturing biomass burning episodes in Southern Africa now should be resolved. The dry period BTs are clearly overlapping with FIRMS fire spots. We furthermore note good agreement between the BTs at the two arrival heights at 100 and 500 m.a.g.l., adding to our confidence of air mass history representativeness. These air mass transport pathways are also in better agreement with the description for RCO provided in DeWitt et al. (2019). Finally, we note that it is re-assuring that the source characteristics present in our chemical and isotope data now are in better agreement with air mass history.

**We have now replaced the old Figure 1 with the new plot with 100m arrival heights (R1), and the 500m arrival height figure (R2) is the new Figure S1 in the SI.**

2.) Monte Carlo Simulations

We agree that the details regarding the MCMC methods should be more comprehensive. We address the topics of convergence and general description, and comparison of observational isotope signatures and back-calculated values here. This discussion is further elaborated upon in the section 3.) on endmember variability.

MCMC Convergence

The Monte Carlo-based technique used here is based on our method described in detail in Andersson et al. (2015). Based on a Bayesian statistical problem formulation, this method will provide robust source quantification and uncertainty estimation, given the underlying probabilistic assumptions and endmember distributions. However, we agree that we have omitted important details regarding the details on this method. As described below, we have now chosen to implement a slightly more advanced source apportionment model, but the generic MCMC parameters remain the same. See added text below.

'The source fractions were computed using numerical Markov chain Monte Carlo simulations, implemented in Matlab, ver. 2015b, using 1000.000 iterations with a burn-in (initial search phase) of 10.000 and a data thinning of 10 (removing step-wise correlations). The stochastic perturbation parameter was adjusted as to obtain an acceptance ratio of 0.23, which has been suggested to be optimal for Metropolis-Hastings algorithms (Roberts et al., 1997). For this set-up, the variability in the numerically estimated parameters, e.g., the standard deviation of the relative source fraction, is lower than 1% of the mean value, suggesting good convergence (Winiger et al., 2017)'

**Line 9 Lines 207-213**

Mass balance-based source apportionment

Overall, we think the back-calculation of observed isotope signatures from the estimated source fractions is an interesting point. However, since mass-balance source apportionment is an inverse technique, error propagation is inherently non-linear, e.g., new version of Eq. (1):

$$f_{bio} = \frac{\Delta^{14}C_{sample} - \Delta^{14}C_{fossil}}{\Delta^{14}C_{bio} - \Delta^{14}C_{fossil}}$$

Furthermore, since we compute source fractions there is a correlation between the central value the variability. Taken together, isotope-values back-calculated from the estimated fraction is theoretically not expected to agree when the variability is large (see, e.g., Andersson, 2012). In fact, the estimated source fractions will tend to equal proportions as a function of increasing endmember variability; the sources become indistinguishable in the limit of very large uncertainties.

After careful consideration of the Reviewer comments regarding endmember uncertainties we have decided to implement a more in-depth Bayesian isotope mass-balance model Martens et al., 2019), described below.

The comparisons between observational and back-calculated isotope ratios are therefore presented in this context, Figs. R5 and R6.

**Figures R5 and R6 combine to a new SI figure 2. And a corresponding comment in the main manuscript:**

'Back-calculating the isotope signatures from the computed source fractions from the MCMC-simulations essentially reproduce the Keeling relations relative to 1/TC (Figs. 5 and S2).'

**Page 15 Lines 388-390**

3.) Endmember variability

An alternative source apportionment model

The isotope endmembers used in the present study are what is essentially measured at 'the tailpipe' of an emission source, and is strongly affected by, e.g., combustion efficiency and the isotope signature of the fuels. This introduce a large variability in the data. However, this large variability is not expected in the atmosphere, where mixing will average the signal from a given source type, e.g., a savanna fire, or source fuel, e.g., $C_4$-plants, and the values will tend to the mean, including kinetic isotope effects (KIE). Thus, source apportionment should therefore ideally be conducted using such averaged signals. However, we do not have this type of data, and estimating the degree of averaging is not straight-forward a priori. If, on the other hand, one can use correlations between the data points, a means for constraining the effective endmember variability at the measurement site can be obtained. Such correlations may be w.r.t. time, concentrations or other parameters.

In the present study, we find that the $\Delta^{14}C$ is well correlated ($R^2 = 0.85$, $p<0.01$) with 1/TC - the 'Keeling relation', Fig. R3 (original Figure 4C), while the correlation of $\delta^{13}C$ vs 1/TC is weaker ($R^2 = 0.56$, $p<0.1$), Fig. R4. The correlation with $\Delta^{14}C$ is unambiguous in the sense that $\Delta^{14}C$ is not affected by kinetic isotope effects, and the endmember values are well-constrained: it directly reports on the relative contributions of biomass/biogenic vs fossil contributions. We thus know that the source-relation exhibited in the $\Delta^{14}C$ data is also present in the $\delta^{13}C$ data, but the weaker $\delta^{13}C$ vs 1/TC trend is due larger endmember variability, and potential kinetic isotope effects. These relations can be used a means for including data correlations in Bayesian MCMC-based source apportionment; accounting for the effects of endmember averaging during air mass transport. Indeed, we have developed such method, with the theoretical basis presented in detail in Martens et al. (2019). This model is essentially an extension of the method used in the original submission: the endmember representation remains the same, but we add the correlations with 1/TC. We emphasize that since the $\Delta^{14}C$ vs 1/TC correlation is stronger, this will impose stronger source constraints than the $\delta^{13}C$ vs 1/TC relation; the strength of the correlation is naturally incorporated within this framework, e.g., compare Figures R3 and R4 with the corresponding Figure R6 and R7.

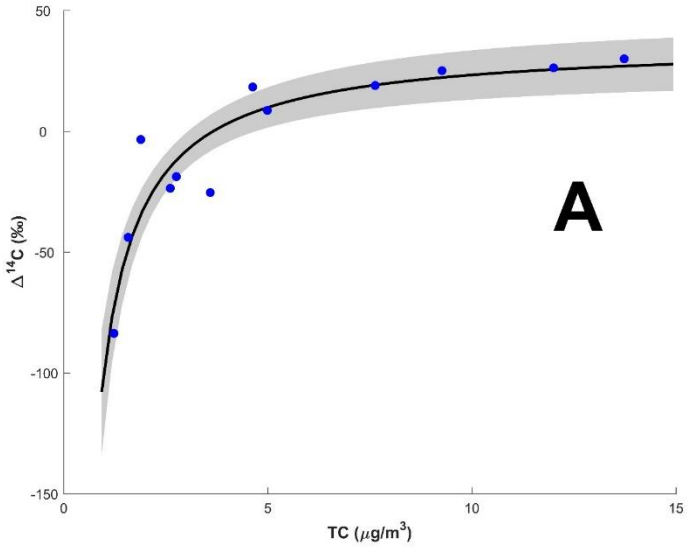


**Figure R3** MCMC fit of $\Delta^{14}C$ vs TC.

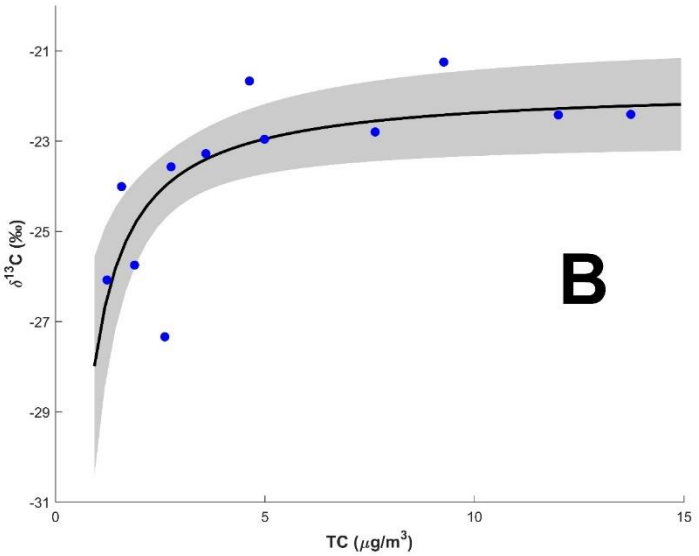


**Figure R4** MCMC fit of $\delta^{13}C$ vs TC.

**Figures R3 and R4 are now Panels A and B in the new Figure 4 in the revised manuscript.**

The statistical strength of the method of Martens et al. compared to the method used in the original submission is illustrated by the number of fitting parameters used in the analysis. In the original submission (where no correlations between data points are used) we fit 24 independent parameters (noting that $f_{C3} + f_{fossil} + f_{C4} = 1$; two independent variables) to 24 data points (12 $\Delta^{14}C$ and 12 $\delta^{13}C$). In the 'Keeling method' we fit 4 independent parameters (2 for the slope and 2 for the intercept of the line) to 24 data points.

In addition, we have conducted a sensitivity analysis of the new source apportionment approach w.r.t. the number of data points included in the calculated. To compare with the scenario where all data points are used, we computed scenarios where only every third point is used (3 scenarios, starting at data point 1, 2 and 3, respectively). We find that the number of data points has a strong influence (as expected) on the computed results, and that the uncertainties on average double in the 'every-third' scenarios. We have added a new Figure S3 (R5), displaying the comparison, and the following text in the R&D:

'To check influence of the number of data points used in the Keeling-based MCMC, we computed comparative scenarios where every third data point was used (starting at data point 1, 2 and 3 respectively) (Fig S3). The standard deviations for the calculated $f_{C3}$ are on average doubled when only every third point are used (5% vs 10%), showing how correlations between multiple data points aids in constraining the sources'

**Page 15 Lines 390-394**

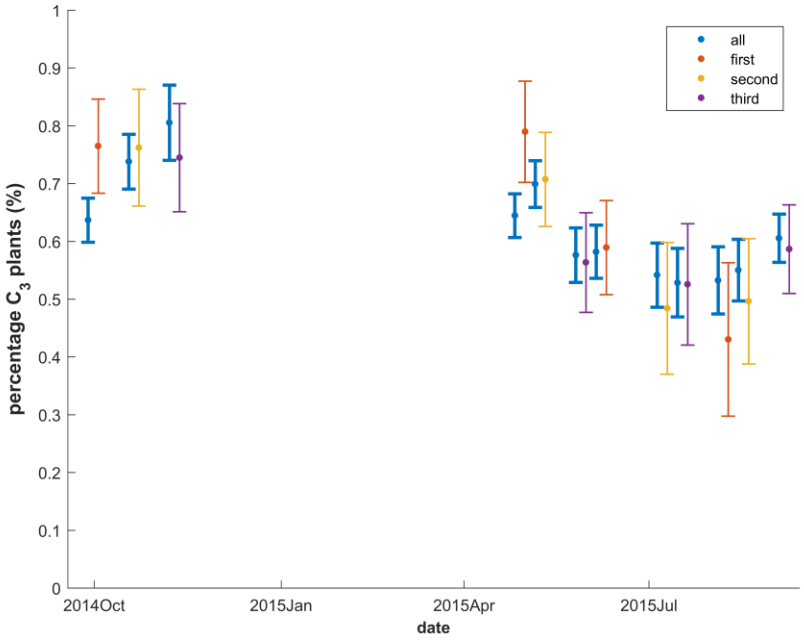


**Figure R5** Sensitivity of the Keeling-based Bayesian MCMC source apportionment approach w.r.t. number of data points in the calculation. The fraction $C_3$-plants is plotted vs time. In blue, the results from using all 12 data pairs (errorbars: mean ± stdev). The orange, yellow and purple lines show calculations using every third data point, starting from data point 1, 2 and 3, respectively. The results from every third data points are shifted slightly in time (to the right) for visual clarity.

As we believe that this method is more statistically and physically sound for the present analysis, we implement this approach. For discussion of the results of this methodology, see below discussion on endmember sensitivity analysis.

We have replaced the old model description in the M&M section with:

'The vegetation in SSA may be divided into two main photosynthetic classes: $C_3$-plants and $C_4$-plants, see discussion in Section 3.5. These two groups have distinct $\delta^{13}C$-signatures, allowing isotope-based separation. We may then resolve three source classes by combining $\Delta^{14}C$ and $\delta^{13}C$: $C_3$-plants, $C_4$- plants and fossil, through isotopic mass-balance (Andersson et al., 2015):

$$\begin{pmatrix} \Delta^{14}C(i) \\ \delta^{13}C(i) \\ 1 \end{pmatrix} = \begin{pmatrix} \Delta^{14}C_{C3} & \Delta^{14}C_{fossil} & \Delta^{14}C_{C4} \\ \delta^{13}C_{C3} & \delta^{13}C_{fossil} & \delta^{13}C_{C4} \\ 1 & 1 & 1 \end{pmatrix} \begin{pmatrix} f_{C3}(i) \\ f_{fossil}(i) \\ f_{C4}(i) \end{pmatrix} \quad (2)$$

Endmember variability may significantly influence the calculated source fractional contributions (Andersson, 2011). For a discussion on the specific endmember ranges used here, see Section 3.5.

In Eq. (2) the isotopic data is treated as independent. However, here we find that there is a dependence between the isotope ratios and the TC concentrations, such that $\Delta^{14}C(i) \sim A/TC(i) + B$, where A and B are constants, and i is the sample index (Fig. 5). This is known as a Keeling relation, and is discussed in more detail in Section 3.4. The relation holds for both $\Delta^{14}C$ ($R^2$=0.85, $p<0.01$) and $\delta^{13}C$, while the correlation is weaker for $\delta^{13}C$ ($R^2$=0.55, $p<0.1$). A method for using correlations within the framework Bayesian source apportionment has recently been developed (Martens et al., 2019). The rationale is based on both statistical concepts and the averaging expected from atmospheric mixing. The endmember ranges used in the calculations are from isolated sources, but during long-range transport the variability within a given source, e.g., savanna fires, will be reduced. Using correlations between data points, a means for accounting for the mixing is obtained, and more realistic source fraction estimates are obtained. When using the estimated source fractions to back-calculate the isotope signatures, the agreement is good compared with direct fits (Fig. 5 and Fig. S2). A sensitivity analysis is discussed in section 3.5 (Fig. S3)

To account for the correlations in the data-set we therefore add a second constraint in the source apportionment calculations, based on the relation to the TC concentrations:

$$\begin{pmatrix} f_{C3}(i) \\ f_{fossil}(i) \\ f_{C4}(i) \end{pmatrix} = \frac{1}{[TC(i)]} \cdot \begin{pmatrix} f_{C3,slope} \\ f_{fossil,slope} \\ f_{C4,slope} \end{pmatrix} + \begin{pmatrix} f_{C3,intercept} \\ f_{fossil,intercept} \\ f_{C4,intercept} \end{pmatrix} \quad (3)$$

Where we, instead of fitting a source vector ($f_{C3}$, $f_{fossil}$, $f_{C4}$) for each individual data pair, fit two vectors: a slope and an intercept of the line, to all data points. This clearly holds the advantage of have fewer fitting parameters. We emphasize that the strength of the correlation of the isotope signatures relative to 1/TC is naturally incorporated into this relation, such that lower correlation of $\delta^{13}C$ w.r.t 1/TC impose weaker constraints on the calculated source fractions, compared to $\Delta^{14}C$.'

**Pages 7-9 Lines 178-206**

Observational vs estimated isotope signatures

To address the Reviewers' comment on comparing the original isotope data with back-calculated parameters, we here present these using the newly implemented Bayesian MCMC model plotted w.r.t. the TC concentrations, Figures R5 and R6. In we see that the estimated $\delta^{13}C$ parameters from the MCMC-based source apportionment strategy essentially replicates Figure R3 and R4, suggesting good agreement, despite the non-linearity of inversion, discussed above.

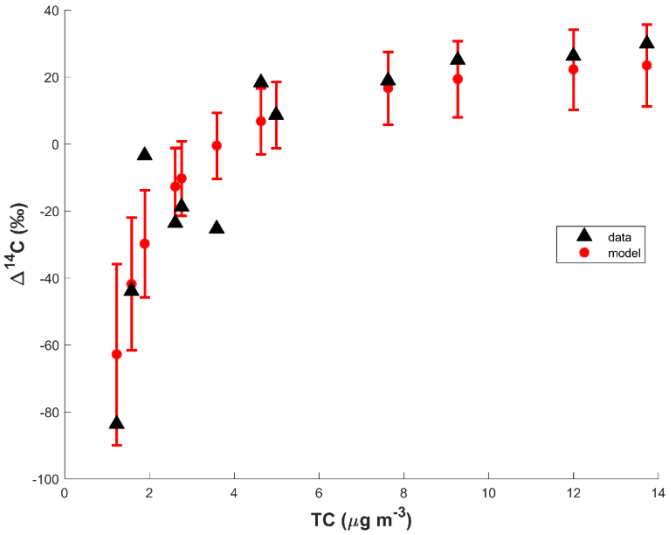


**Figure R6** Comparison of observed carbon isotope signatures (black triangles) for TC and values back-calculated from the MCMC-estimated source fractions using the 'best endmember scenario' (red circles with errorbars). Panel A. $\Delta^{14}C$ vs TC. Panel B. $\delta^{13}C$ vs TC.

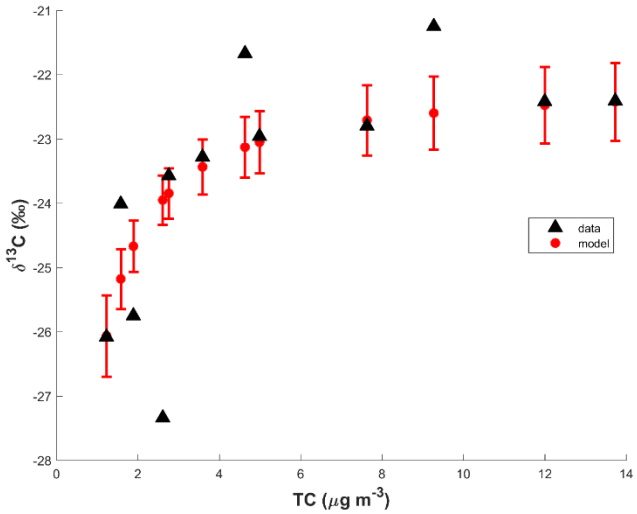


**Figure R7.** Comparison of observed carbon isotope signatures (black triangles) for TC and values back-calculated from the MCMC-estimated source fractions using the 'best endmember scenario' (red circles with errorbars). Panel A. $\Delta^{14}C$ vs TC. Panel B. $\delta^{13}C$ vs TC.

Figures R6 and R7 combine to a new Figure S2, and we have added the following text to the main manuscript:

'When using the estimated source fractions to back-calculate the isotope signatures, the agreement is good compared with direct fits (Fig. 5 and Fig. S2).'

**Page 8, Lines 195-197**

Endmember sensitivity tests

The reviewer raises concerns w.r.t. endmember variability and representativity. Here we address four different endmember scenarios, see also responses to specific points below:

a. *The 'original' best scenario:*
   $\delta^{13}C_{C3}$ = -27.1 ± 2.2 ‰; $\delta^{13}C_{fossil}$ = -25.5 ± 1.3 ‰; $\delta^{13}C_{C4}$ = -16.6 ± 2.2 ‰
b. *The 'no-KIE $C_4$' scenario:*
   $\delta^{13}C_{C3}$ = -27.1 ± 2.2 ‰; $\delta^{13}C_{fossil}$ = -25.5 ± 1.3 ‰; $\delta^{13}C_{C4}$ = -13.1 ± 1.2 ‰
   Where the $\delta^{13}C$ endmember range of $C_4$ is not affected by any KIE depletion.
c. *The 'max-KIE $C_4$' scenario:*
   $\delta^{13}C_{C3}$ = -27.1 ± 2.2 ‰; $\delta^{13}C_{fossil}$ = -25.5 ± 1.3 ‰; $\delta^{13}C_{C4}$ = -19.0 ± 2.2 ‰
   This scenario corresponds to the point where the estimated $f_{C4}/(f_{C4} + f_{C3})$ = 0.64 in the limit TC $\rightarrow\infty$; the signature expected from pure savanna fires.
d. *The 'depleted fossil' scenario:*
   $\delta^{13}C_{C3}$ = -27.1 ± 2.2 ‰; $\delta^{13}C_{fossil}$ = -28.5 ± 1.3 ‰; $\delta^{13}C_{C4}$ = -16.6 ± 2.2 ‰
   In this scenario we shifted the fossil average by -3 ‰. There is no real quantitative argument for this depletion, other than it represents a large shift.

a. The original scenario

In this scenario we use the endmember ranges presented in the original submission, but with the source apportionment strategy from Martens et al. (2019), Fig. R8 is the new Figure 7. Compared to the original submission, we find that this method provides a significantly larger separation between the relative $C_3$ and $C_4$ plant contributions, with a suppression of the estimated uncertainties, see also above discussion regarding a sensitivity of the new MCMC strategy w.r.t. number of data points.

In the limit of TC approaching infinity, $f_{C4}/(f_{C4} + f_{C3})$ = 0.47 for this scenario. Since the $f_{C4}/(f_{C4} + f_{C3})$-value for East African savannas is ~ 0.64, this limit would correspond to 74% savanna contributions.

This scenario is what we consider to be the most likely, as it is represents the average of the no KIE scenario and the maximum KIE-induced $^{13}C$ depletion observed (-7‰).

New text in the main manuscript:

‘Accounting for such effects in source apportionment is a challenge, especially since the reported values are ranges and not mean and variability, and thus are highly influenced by potential outliers. We here use a method discussed in Andersson et al. (2015) to address the issue of statistical analysis of ranges by assuming that the total range corresponds to the 95% confidence intervals of a normal distribution. This corresponds to the range of 4 times the standard deviation, yielding $\sigma$ = 7/4‰, while the mean is -7/2‰. Combining this with the variability of the of pure $C_4$-plants we obtain: $\delta^{13}C_{C4}$: -16.6 ± 2.2‰, where $\sigma^2 = 1.2^2 + (7/4)^2$ ‰$^2$. These values are also what is obtained by numerical estimation of the convolution of a normal distribution ($\mu$ = -16.6, $\sigma$ = 1.2‰) with a uniform distribution ([-7, 0] ‰), adding to the strength of statistical representation.’

**Page 14-15 Lines 369-377**

**Table S2 is updated accordingly.**

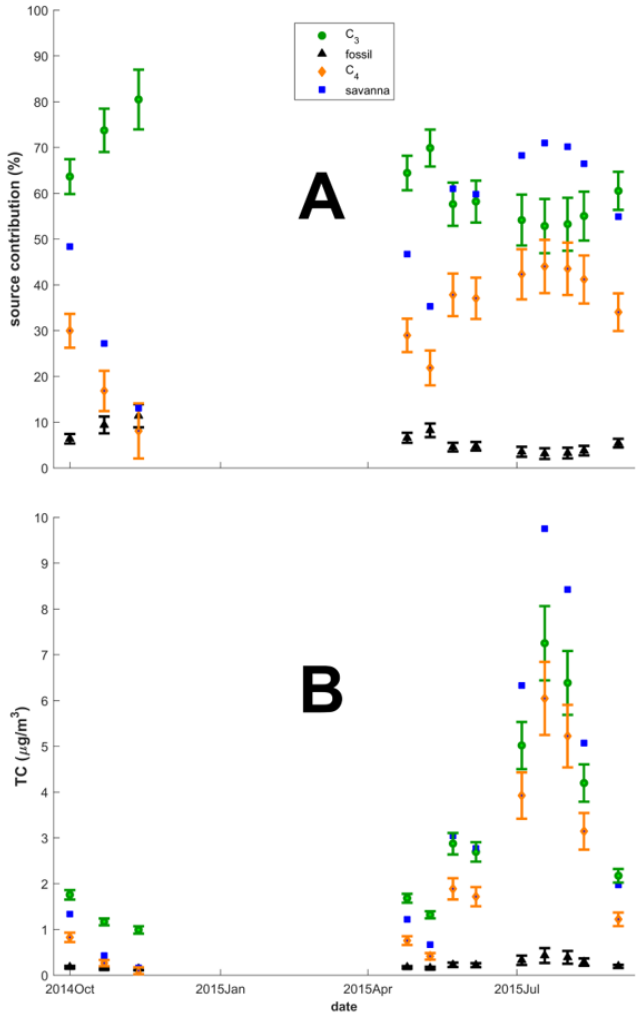


**Figure R8** Estimated source fractions and source-segregated TC concentrations with the **original endmember scenario.**

b. The no KIE scenario

This scenario corresponds to the case where the $\delta^{13}C_{C4}$ of aerosols is not associated by any $^{13}C$-depletation by KIE. Consequently, it is a 'minimum $C_4$' scenario. In the limit of TC approaching infinity, $f_{C4}/(f_{C4} + f_{C3})$ = 0.36 corresponding to 55% savanna. This is thus the lower bound for savanna contributions int the TC→∞ limit, as is apparent in Fig R9. However, it is not a likely scenario, as there are known KIEs in aerosols emitted from $C_4$ incomplete combustion.

**Figure R9 is a new Figure S5, and the results are added in the new Table S4.**

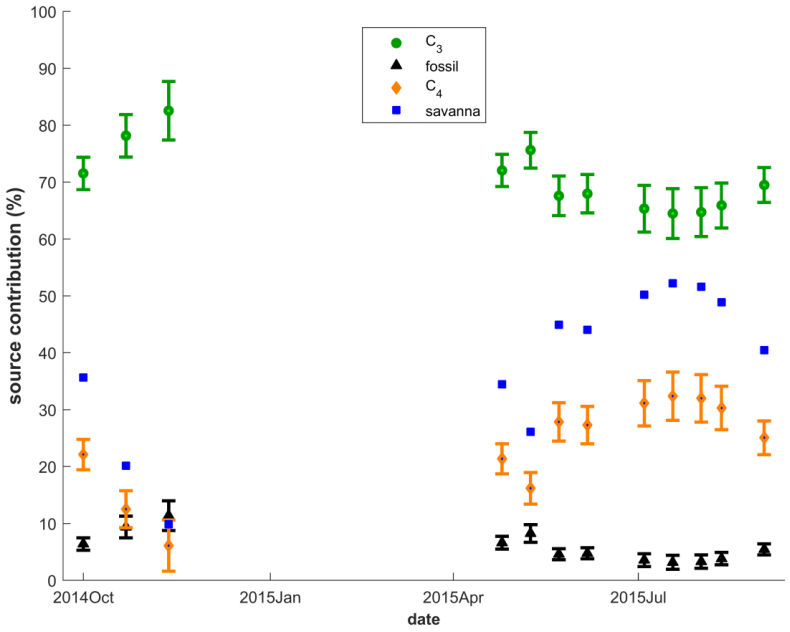


**Figure R9** Estimated source fractions with the **no-KIE endmember scenario.**

c. The max-KIE scenario

In this scenario we use the $\delta^{13}C_{C4}$ endmember values that corresponds to the $f_{C4}/(f_{C4} + f_{C3})$ observed in East African savannas, 0.62, Fig. R9. The KIE is -5.9‰ relative to pure $C_4$-plants, and we thus would have 100% savanna fire contributions in the TC→∞ limit. As for point c, this is an extreme limit scenario and is less likely than the original 'best' scenario.

**Figure R10 is a new Figure S4, and the results are added in the new Table S3.**

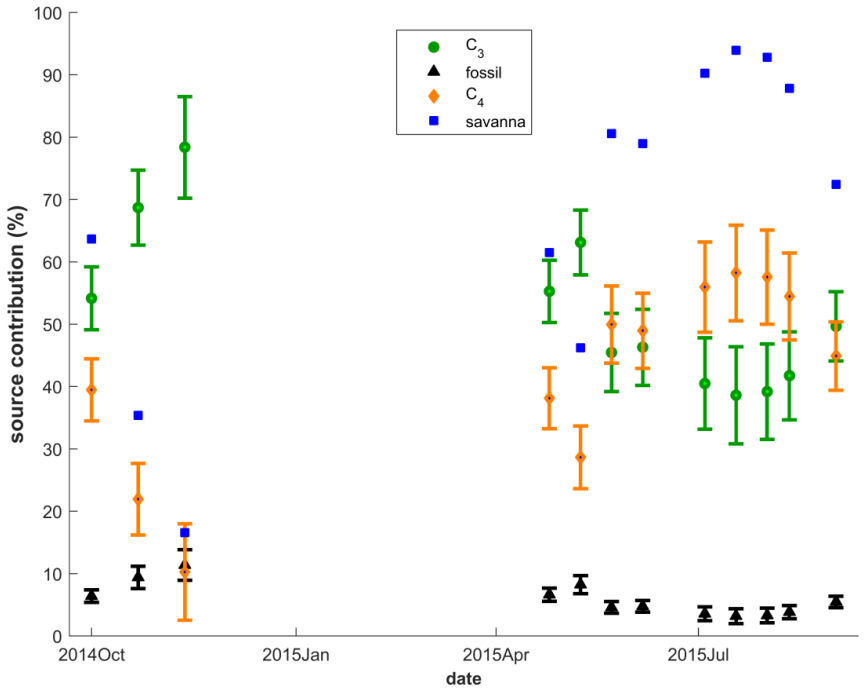


**Figure R10** Estimated source fractions with the **max-KIE endmember scenario**.

d. The depleted fossil scenario

In this scenario we shift the fossil $\delta^{13}C$ endmember by -3‰, Fig. R11. In this scenario the fossil fractions shift by less than 5%. This is not surprising, as the main determinant of the fossil contributions is the $\Delta^{14}C$ data Given the low overall fossil contributions (15%<), this shift in $\delta^{13}C_{fossil}$ does not propagate into the differentiation between $C_3$ and $C_4$ plants. Overall, we conclude that the set-up is not sensitive to the fossil $\delta^{13}C$ endmember for the present data.

**Figure R11 is a new Figure S6, and the results are added in the new Table S5.**

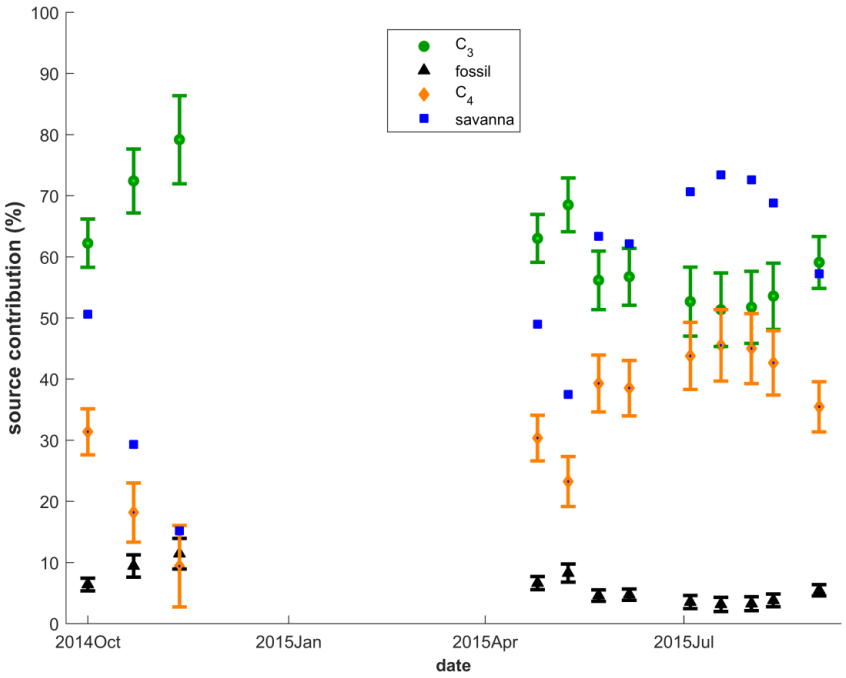


**Figure R11** Estimated source fractions with the **depleted fossil endmember scenario**.

Overall, we conclude that:

1. That, as expected, the value of the $C_4$ $\delta^{13}C$ influence the estimated fractional $C_4$ contributions, such that the larger the KIE the larger the fraction $C_4$.
2. The estimated source fractions are insensitive to the $\delta^{13}C$-fossil endmember.
3. The sensitivity analysis from the maximum and minimum KIE $C_4$ $\delta^{13}C$ endmember shows that the savanna contributions may span 55% to 100%. However, the original best scenario is the most un-biased representation.

**We have added the following text to the R&D:**

'Since the $\delta^{13}C$ endmembers for, in particularly $C_4$-plants, are not well-constrained, we also employed a sensitivity analysis w.r.t. endmembers and the potential influence of KIE (Tables S2 – S5 and Figs. S4 – S6). In addition to the above discussed best estimate scenario, we tested two $\delta^{13}C_{C4}$ scenarios: a 'minimum KIE scenario' with zero KIE ($\delta^{13}C_{C4}$ -13.1±1.2‰) and a 'maximum KIE scenario', with a depletion by 5.9‰ ($\delta^{13}C_{C4}$ -19.0±2.2‰). The maximum KIE scenario was established such as the $f_{C4}/(f_{C4}+f_{C3})$-ratio would be 62% as TC approach infinity, and thus 100% savanna contributions, see Eq. (4). As expected, these scenarios significantly shift the estimated relative $C_4$ contributions, resulting in a total range of the sample period averages of 24% (min-KIE; min 6% max 32%) to 42% (max-KIE; min 10%, max 58%), thus providing lower and upper bounds (Figs. S4 and S5 and Tables S3 and S4). The corresponding value for

our best estimate is 32% (max 44%, min 8%). In addition, we investigated a scenario with a 3‰ depletion of the fossil endmember ($\delta^{13}C_{fossil}$ -28.5±1.3‰). Since the fossil contribution is overall low as determined by $\Delta^{14}C$, and since $\Delta^{14}C$ constrains the fossil contribution independently of the $\delta^{13}C$ data, this shift has no significant influence on the computed source fractions 6% (max 11%, min 3%) (Fig. S6 and Table S5). Overall, we stress that these three sensitivity test scenarios represent extreme limits, and the a priori least biased scenario is the initially outlined best scenario.'

**Pages 15-16 Lines 395-410**

4. Responses to specific comments

*Line 235. Out-gassing SO2 emissions can contribute very significantly to regional sulphate levels even without recognised volcanic activity (Ovadnevaite et al. 2009).*

We agree. We now write.

'RCO is situated not far away from the Nyiargongo and Nyamuragria Volcanoes in eastern Democratic Republic of Congo. High spatial resolution (13x24km$^2$) satellite-monitoring of the $SO_2$ levels show a near-constant emissions from these volcanoes over the time period covering the present campaign, likely affecting the observed sulfate levels (Barrière et al., 2017). Here we observe a spike in sulfate levels (~ 5µg m$^{-3}$) during the week starting of the 13$^{th}$ of June 2015 (Fig. 2), but with no clear linkage to an increase in volcanic $SO_2$ emissions'

**Page 11 Lines 259-264**

*Line 246. Authors may also consider that OC/EC ratio is very dependent on the combustion stage - flame fires versus smouldering fires.*

This is certainly true. We now emphasize this fact:

'The OC/EC-ratio is sometimes used as a marker for biomass burning, but is highly influenced by burning conditions such as flaming or smoldering fires.'

**Page 11 Lines 271-272**

*Line 321. d13 fossil ratio is very much region dependent and needs to be better constrained or uncertainty increased. It is possible that African liquid fossil fuel isotopic signatures are around -25, but it can be as low as -29 in other regions and, therefore, should be much better constrained or proven or uncertainty increased.*

We agree that there can be high regional variability, emphasizing the crucial need to incorporate endmember variability in source apportionment calculations. In earlier publications, we have recognized

that the $\delta^{13}C$ for Russian liquid fossil fuels, is more in the range of -31 per mille, while the majority of other fuels are in the presently used range (Winiger et al., 2017). In the above sensitivity test we show that the exact value of the fossil endmember has little influence on the presently evaluated source fractions, Fig R10.

**See above revisions in the new manuscript.**

*Line 328. Why the uncertainty of of C4 isotopic signature is twice smaller than of C3 plants? It also contradicts Figure 5 where C4 signature is ~16.5+/-2. That seems to be biased low as C4 signatures are more in the region of -16 to -10 (something like -13+-3). C4 signatures need to be much better constrained which will have significant impact on source contribution and associated uncertainty.*

A priori, there is no clear reason as to why the variability of either $C_3$ or $C_4$ should be smaller, larger or similar. However, one may use evolutionary/ecological arguments to explain why the variability of $C_4$ might be expected to be smaller: $C_4$-plants branched off from the $C_3$-plants stem in the evolutionary tree to colonize a comparably specific ecological niche: hot and dry conditions (e.g., savannas). $C_3$-plants, on the other hand, are abundantly present in a much wider array of ecological niches, including savannas, boreal forests, marine environements etc. Adaption to a wide array of environmental conditions is expected to affect the $\delta^{13}C$, either evolutionary (genetically) or physiologically, such that the variability will increase.

No citation is provided for the number -13+-3. Here, we have cited extensive reviews (based on 'hundreds of papers') on the subject of the $\delta^{13}C$-values of $C_4$-plants, arriving at the value used here (Bender et al., 1971; O'Leary et al., 1988; Turekian, 1998). However, the main uncertainty here lies not in the $\delta^{13}C$-values themselves, but in the kinetic isotope effects associated with combustion and transformation into aerosols. Here, the literature is scarce, and mainly provide ranges, which are hard to evaluate statistically, as they may be very biased towards outliers. **See above changes in the manuscript**

*Line 342. The result is highly contentious. Why only C4 plants burning are dominant during dry season? While only C3 plants contribute to wet season SOA? The statement contradicts Figure 6 where C4 and C3 contribution is about equal even during dry season.*

We have significantly changed this section, see above responses.

*Figure 6 does not fit discussion and seem to be interpreted very subjectively.*

See above discussion

*Outlook section The authors should not discuss implications beyond presented data. Cloud brightening and broad climatic implications are not supported by the study data and seem to be out of place.*

We agree to some extent, and have reduced the Outlook section, and removed, e.g., the discussion on cloud brightening. However, we do maintain that a broader discussion on implications is warranted in an outlook section (it is not a summary or conclusions part).

*Figure 4. Uncertainty error bars are absent in the Figure*.

The uncertainties for $\Delta^{14}C$ are below 50‰ and ~ 0.2‰ for $\delta^{13}C$. We have added this information to the figure legend for visual clarity.

## REFERENCES FOR REVIEWER COMMENTS


Andersson, A.: A systematic examination of a random sampling strategy for source apportionment calculations. Sci. Tot. Environ. 412-413, 232-238, doi: 10.1016/j.scitotenv.2011.031, 2011.

Andersson, A., Deng, J., Du, K., Zheng, M., Yan, C., Sköld, M., Gustafsson, Ö.: Regionally-varying combustion sources of the January 2013 severe haze events over Eastern China. Environ. Sci. Technol. 49, 2038-2043, doi: 10.1021/es503855e, 2015.

Bender, M.M.: Variations in the $^{13}C/^{12}C$ ratios of plants in relation to the pathway of photosynthetic carbon dioxide fixation. Phytochem. 10, 1239-1244, doi: 10.1016.S0031-9422(00)84324-1, 1971.

Budhavant, K., Andersson, A., Bosch, C., Kruså, M., Kirillova, E.N., Sheesley, R.J., Safai., P.D., Rao, P.S.P., Gustafsson, Ö.: (2015) Radiocarbon-based source apportionment of elemental carbon aerosols at two South Asian receptor observatories over a full annual cycle. Environ. Res. Lett. 10, doi: 10.1088/1748-9326/10/6/064004.

Fang, W., Du, K., Andersson, A., Zing, Z., Cho, C., Kim, SW., Deng, J., Gustafsson, Ö.: (2018) Dual-Isotope Constraints on Seasonally Resolved Source Fingerprinting of Black Carbon Aerosols in Sites of the Four Emission Hot Spot Regions of China. J. Geophys. Res. doi: **10.1029/2018JD028607**.

Martens, J., Wild, B., Pearce, C., Tesi. T., Andersson, A., Bröder, L., O'Regan, M., Jakonsson, M., Sköld, M., Gemery, L., Cronin, T.M., Semiletov, I., Dudarev, O.V., Gustafsson, Ö.: (2019) Remobilization of Old Permafrost Carbon to Chukchi Sea Sediments During the End of the Last Deglaciation. Glob. Biogeochem. Cyc. 33, 2-14, doi: **10.1029/2018GB005969**.

O'Leary, M.H.: Carbon isotopes in photosynthesis. Bioscience 38, 328–36, doi: 10.2307/1310735, 1988.

Roberts, G.O., Gelman, A., Gilks, W.R.: (1997) Weak convergence and optimal scaling of random walk Metropolis algorithms. Ann. Appl. Prob. 7, 110-120.

Turekian, V. C., Macko, S., Swap, R. J. and Garstang, M.: Causes of bulk carbon and nitrogen isotopic fractionations in the products of vegetation burns: laboratory studies. Chem. Geol. 152, 181-192, 10.1016/S0009-2541(98)00105-3, 1998.

Winiger, P., Andersson, A., Eckhardt, S., Stohl, A., Semiletov, I.P., Dudarev, O.V., Charkin, A., Shakova, N., Klimont, Z., Heyes, C., Gustafsson, Ö.: (2017) Siberian Arctic black carbon sources constrained by model and observation. Proc. Nat. Acad. Sci. doi: **10.1073/pnas.1613401114**.

Winiger, P., Barrett, T.E., Sheesley, R.J:, Huang, L., Sharma, S., Barrie, L.A., Yttri, K.E., Evangeliou, N., Eckhardt, S., Stohl, A., Klimont, Z., Heyes, C., Semiletov, I.P., Dudarev, O.V., Charkin, A., Shakhova, N., Holmstrand, H., Andersson, A., Gustafsson, Ö.: Source apportionment of circum-Arctic atmospheric black carbon from isotopes and modelling. Sci. Adv. 5, doi: 10.1126/sciadv.aau8052, 2019.

# Seasonal source variability of carbonaceous aerosols at the Rwanda climate Observatory

August Andersson[1], Elena N Kirillova[1,2], Stefano Decesari[2], Langley DeWitt[3], Jimmy Gasore[3,4,5], Katherine E Potter[3], Ronald G Prinn[3], Maheswar Rupakheti[6], Jean de Dieu Ndikubwimana[4], Julius Nkusi[4], Bonfils Safari[5].

[1] Department of Environmental Science and the Bolin Centre for Climate Research, Stockholm University, SE-10691 Stockholm, Sweden

[2] Institute of Atmospheric Sciences and Climate-ISAC, National Research Council of Italy, Bologna, Italy

[3] Center for Global Change Science, Massachusetts Institute of Technology, Cambridge, MA, USA

[4] Climate Secretariat, Ministry of Education, Kigali, Rwanda

[5] Physics Department, School of Physics, College of Science and Technology, University of Rwanda, Kigali, Rwanda

[6] Institute for Advanced Sustainability Studies (IASS), Potsdam, Germany

**Correspondence:** August Andersson (august.andersson@aces.su.se)

## Abstract

Sub-Saharan Africa (SSA) is a global hotspot for aerosol emissions, affecting the regional climate and air quality. In this paper we use ground-based observations to address the currently large uncertainties in source-resolved emission estimation of carbonaceous aerosols. Ambient fine fraction aerosol were collected on filters at the high altitude (2590 m.a.s.l.) Rwanda Climate Observatory (RCO), a SSA background site, during dry and wet seasons in 2014 and 2015. The concentrations of both carbonaceous and inorganic ion components show a strong seasonal cycle, with highly elevated concentrations during the dry season. Source marker ratios, including carbon isotopes, show that the wet and dry seasons have distinct aerosol compositions. The dry season is characterized by elevated amounts of biomass burning products, approaching ~ 95% for carbonaceous aerosols. An isotopic mass-balance estimate show that the amount of the carbonaceous aerosols stemming from savanna fires may increase from 0.2 μg/m$^3$ in the wet season up to 10μg/m$^3$ during the dry season. Taken together, we here quantitatively show that savanna fire is the key modulator of the seasonal aerosol composition variability at the RCO.

## 1. Introduction

Sub-Saharan Africa (SSA) currently faces major challenges for sustainable development, including industrial development, agriculture, fresh water supply, climate change, energy resources and air pollution (IPCC 2014; UNDP, 2018). Either directly, or indirectly, these challenges are linked to aerosol emissions. Aerosols offset the ongoing regional climate warming in SSA, shift monsoon and precipitation patterns, and are detrimental for air quality (IPCC 2013; WHO 2016). Ambient air pollution in SSA is estimated to cause 563.000 premature deaths annually, making it one of the main causes for mortality in the region (Bauer et al., 2019). However, the level of scientific understanding of the overall health- and climate impact is still low, owing to the complex aerosol lifecycle, where emissions, transformations and sinks are associated with large uncertainties, in particular given their vast physical and chemical complexity. A major limiting factor for improving our understanding of these effects in SSA are the limited number of in situ observations (Williams, 2007; Cais et al., 2011; Kulmala, 2018; López-Ballesteros et al., 2018).

A major source of aerosol emissions in SSA are dry season regional fires, clearly visible from space (Fig. 1). These are occasionally ignited naturally by lightning strikes, but are mainly lit by humans. There is evidence that slash-and-burn agriculture in SSA has been a common practice for thousands of years (Bird and Cali, 1998; Archibald et al., 2012). This long-term anthropogenic perturbation is a significant modulator of current ecosystem structure. A number of studies have specifically focused on characterizing emissions of aerosols and gases from African fires, e.g., the Southern African Regional Science Initiative Project (SAFARI 2000), conducted between 1999 to 2001 (Swap et al., 2003). Ground- and airborne chemical characterization from this and other campaigns suggest a rather distinct aerosol chemical composition, including elevated BC, $K^+$ and $NO_3^-$ concentrations (Table 1).

Carbonaceous aerosols, often quantified as total carbon (TC), are generally divided into two main components: black carbon (BC; here we use elemental carbon (EC) to quantify the amounts of BC) and organic carbon (OC). Although overlapping to some extent, these two pools generally have distinct atmospheric lifecycles and environmental effects. Formed from incomplete combustion, sunlight-absorbing BC contributes to regional warming and is a particularly health detrimental component in air pollution (WHO 2012; WMO/UNEP 2011; IPCC 2013; Bond et al.,

2013). BC is chemically inert to atmospheric reactions, and thus the lifetime is mainly determined by deposition. OC is also emitted from incomplete combustion (however, with different emission factors) but is also of non-combustion origins and is formed in the air through secondary processes. OC is thought to have an overall cooling effect on the climate (IPCC, 2013). Being more chemically reactive, the OC pool to some extent has a more complex atmospheric lifecycle, with continuous heterogenous chemistry, rendering the lifetime dependent on both precipitation and chemical transformations. Emissions from SSA fires are expected to contribute to a significant part of the global TC atmospheric burden (Liousse et al., 2015).

In general, the actual environmental impact of TC on SSA is poorly constrained. Bottom-up emission projections suggests that the TC emissions from SSA are expected to increase rapidly during the coming decades, perhaps reaching 50% of the global burden by 2030 (Liousse et al., 2014). To quantify and evaluate such model predictions, as well as to characterize the overall aerosol composition, it is valuable to conduct measurements at regional background sites. Dual carbon isotope characterization ($\Delta^{14}C$ and $\delta^{13}C$) of TC at background sites in South and East Asia and the Arctic has been shown to be a valuable tool for quantitatively constraining the emissions from different sources (Gustafsson et al., 2009; Andersson et al., 2015; Sheesley et al., 2012; Kirillova et al., 2014; Winiger et al., 2019).

In this paper we present dual carbon isotope constraints of TC, along with chemical characterization of inorganic ions and different carbonaceous pools, from a study conducted at the Rwanda Climate Observatory (RCO), during October 2014 to September 2015. A key objective of the study was to estimate the relative contributions from major TC source categories at this regionally representative site in the SSA. In particular, we investigate the source variability associated with the seasonal variations between prevailing wet and dry monsoon seasons in the region and the contributions from savanna fires.

## 2. Methods and Materials

### 2.1 Field site and regional meteorology

The sampling site, the Rwanda Climate Observatory (RCO), is located on the top of Mt. Mugogo, in mountainous western Rwanda. (1.586° S, 29.566° E, 2590 m above sea level, 5 m.a.g.l.). The

station was established as a collaboration between the Massachusetts Institute of Technology (MIT, USA) and the Rwandan Government in 2013. The station is described in more detail by DeWitt et al. (2019). The station is an Advanced Global Atmospheric Gases Experiment (AGAGE) network site (for full list of instruments see http://agage.mit.edu).

The meteorology of Rwanda is governed by the East African monsoon, with peak rainfalls in in April and November. There are thus two dry seasons, December-January-February (DJF) and the main dry season June-July-August (JAA). The dry seasons in SSA are characterized by extensive biomass burning. During JJA the fires mainly occur to the south of Rwanda (Fig. 1). Savannas are the main biomes in SSA, covering ~ 65% of the landmass, and are the main source of fire emissions (Cahoon et al., 1992). Located in a highly elevated region, Rwanda is, broadly speaking, surrounded by savanna regions, except to the west, where the tropical rainforests of Africa are located.

## 2.2 Filter sampling

Quartz filter samples (Millpore, 150 mm diameter) were collected with a high-volume sampler operating at 30$m^3\,h^{-1}$ using a $PM_{2.5}$ inlet (DH-77, Digitel Inc. Switzerland). Night-time only (1AM to 6AM) was conducted to minimize the effects of local emissions and day-time local atmospheric chemistry and to increase likelihood to capture the regional, free troposphere, signals. This strategy is supported by high temporal resolution investigations of the diurnal cycle of, e.g., BC (DeWitt et al., 2019). Each sample was collected over a period of 7 days. The samples were pre-combusted together with aluminum foil envelopes (400ºC for 5h), and were treated with special attention to minimize contamination. The samples were subsequently shipped to Stockholm University for chemical analysis and isolation for carbon isotope analysis. The samples were stored in freezers both on site and at Stockholm University. Field blanks were collected on a monthly basis. The present campaign covers the period October 2014 to September 2015. However, the period December 2014 to April 2015 is missing due to a lightning strike which damaged the instrument. Thus, this study presents results from analysis of filter samples (in total 25) collected for the periods that cover the beginning of the 2014 fall rainy season (Oct-Nov), the end of the spring 2015 rainy season (April – May) and the dry 2015 summer season (June – September). We jointly refer the October-November 2014 and the April-May 2015 periods as the wet seasons.

## 2.3 Concentrations analysis

The concentrations of elemental carbon (EC – mass-based tracer for black carbon) and organic carbon (OC) were determined using a Sunset Inc. (Tigard, Oregon, USA) thermal-optical instrument using the NIOSH 4050 protocol (Birch and Cary, 1996; Table S1). Pre-treatment using acid fumigation with 1M HCl ensured efficient removal of carbonates. A glucose solution was used to calibrate the FID-response of the instrument, and the long-term performance of the instrument was checked through running of National Institute of Standards and Technology (NIST) Standard Reference Materials (SRM) standards. All the concentrations were blank corrected and the field blank input was on average 2% for OC and 0% for EC. The average relative standard deviation of the triplicate analysis was 5% for OC, 7% for EC.

Water-soluble organic carbon (WSOC) was extracted from filter sub-samples in ultra-pure Milli-Q water by shaking for 1.5 hours. The extracts were filtered using 0.45 µm cutoff PTFE syringe filters (Minisart-SRP 10, Sartorius Stedim biotech, Germany). The concentration of WSOC was quantified in the filtered solutions as the difference between total water-soluble carbon and water-soluble inorganic carbon using a high temperature catalytic oxidation instrument TOC-5000A (Shimadzu, Japan). The samples were neither acidified nor purged, to avoid the loss of volatile organic compounds. The accuracy of the measurement ranges from 7% (70 µg $L^{-1}$) for 1 mg $L^{-1}$ of carbon solution to 3% for concentrations higher than 2 mg $L^{-1}$ of carbon (corresponding to 60 µg $L^{-1}$). All the measurements were blank corrected. WSOC field blanks corresponded to an average 0.5%. The average relative standard deviation of the triplicate analysis was 10%.

The concentrations of water-soluble inorganic anions were determined by ion chromatography using a Dionex ICS-2000 system. Anions were separated using an IonPac AG11 2x50 mm Dionex guard column, IonPac AS11 2x250 mm Dionex separation column and ASRS 300 self-regenerating suppressor. A solution of KOH was used as eluent. Cations were separated using an IonPac CG16 3x50 mm Dionex guard column, IonPac CS11 3x250 mm Dionex separation column and CSRS 300 self-regenerating suppressor. The analysis of cations was performed using 30 mM solution of MSA as eluent. Field blanks constituted on average 3% of $NO^{3-}$, 2% of $SO_4^{2-}$ and 1% of $NH_4^+$ and $K^+$ ion concentrations. The triplicate analysis showed the average relative standard deviation of 2% for $NO^{3-}$ and $K^+$, 5% for $SO_4^{2-}$ and 6% for $NH_4^+$.

## 2.4 Isotope analysis

Approximately every second sample (n = 12) were selected for carbon isotope ($\Delta^{14}C$ and $\delta^{13}C$) analysis of total carbon (TC = OC + EC; Table S1). The filter samples were combusted using the Sunset analyzer (total carbon protocol) and the evolved $CO_2$ was collected in glass vials using a liquid nitrogen cryo-trap (Andersson et al., 2015). The vials were subsequently shipped to the National Ocean Sciences Accelerator Mass Spectrometry (NOSAMS) facility at the Woods Hole Oceanographic Institute (Falmouth, Massachusetts, USA) for analysis of the dual carbon isotope signatures. The $\Delta^{14}C$-signature was measured using accelerator mass spectrometry (AMS), while the $\delta^{13}C$-signature was measured using an Isotope Ratio Mass Spectrometer (IRMS).

## 2.5 Source Apportionment

The $\Delta^{14}C$-signature allows the differentiation between the relative contributions of biogenic/biomass burning and fossil sources. The fraction biogenic/biomass burning ($f_{bio}$) may be calculated using isotopic mass-balance ($f_{fossil} = 1 - f_{bio}$):

$$f_{bio} = \frac{\Delta^{14}C_{sample} - \Delta^{14}C_{fossil}}{\Delta^{14}C_{bio} - \Delta^{14}C_{fossil}} \quad (1)$$

The fossil endmember is -1000‰, as it is completely depleted in $^{14}C$. The biomass endmember is more complex. For annual plants it is fairly straight-forward: the biomass $\Delta^{14}C$-signature equals the $\Delta^{14}C$ value of $CO_2$ for that year (~ +20‰ for 2014/15, Graven, 2015; Turnbull et al., 2017). For more long-lived species (e.g., trees) the $\Delta^{14}C$-signature is the average of the atmospheric $CO_2$ values (weighted by yearly carbon accumulation) over the plants' lifetime. Bottom-up estimation of $\Delta^{14}C_{bio}$ therefore requires information regarding the plant distribution in the area of interest, and the annual bioaccumulation of carbon for the different plants. As an alternative we here use the combined $\Delta^{14}C$-signature of dissolved organic carbon (DOC) in three of the regions' major rivers, Congo, Zambezi and Tana, to obtain a regional $\Delta^{14}C_{bio} = +57 \pm 52$ ‰, which is well in the expected range of a mixture of annual and multi-year plants (Marwick et al., 2015; Wild et al., 2019, Winiger et al., 2019).

The vegetation in SSA may be divided into two main photosynthetic classes: $C_3$-plants and $C_4$-plants, see discussion in Section 3.5. These two groups have distinct $\delta^{13}C$-signatures, allowing isotope-based separation. We may then resolve three source classes by combining $\Delta^{14}C$ and $\delta^{13}C$: $C_3$-plants, $C_4$- plants and fossil, through isotopic mass-balance (Andersson et al., 2015):

$$\begin{pmatrix} \Delta^{14}C(i) \\ \delta^{13}C(i) \\ 1 \end{pmatrix} = \begin{pmatrix} \Delta^{14}C_{C3} & \Delta^{14}C_{fossil} & \Delta^{14}C_{C4} \\ \delta^{13}C_{C3} & \delta^{13}C_{fossil} & \delta^{13}C_{C4} \\ 1 & 1 & 1 \end{pmatrix} \begin{pmatrix} f_{C3}(i) \\ f_{fossil}(i) \\ f_{C4}(i) \end{pmatrix} \quad (2)$$

Endmember variability may significantly influence the calculated source fractional contributions (Andersson, 2011). For a discussion on the specific endmember ranges used here, see Section 3.5.

In Eq. (2) the isotopic data is treated as independent. However, here we find that there is a dependence between the isotope ratios and the TC concentrations, such that $\Delta^{14}C(i) \sim A/TC(i) + B$, where A and B are constants, and i is the sample index (Fig. 5). This is known as a Keeling relation, and is discussed in more detail in Section 3.4. The relation holds for both $\Delta^{14}C$ ($R^2$=0.85, $p<0.01$) and $\delta^{13}C$, while the correlation is weaker for $\delta^{13}C$ ($R^2$=0.55, $p<0.1$). A method for using correlations within the framework Bayesian source apportionment has recently been developed (Martens et al., 2019). The rationale is based on both statistical concepts and the averaging expected from atmospheric mixing. The endmember ranges used in the calculations are from isolated sources, but during long-range transport the variability within a given source, e.g., savanna fires, will be reduced. Using correlations between data points, a means for accounting for the mixing is obtained, and more realistic source fraction estimates are obtained. When using the estimated source fractions to back-calculate the isotope signatures, the agreement is good compared with direct fits (Fig. 5 and Fig. S2). A sensitivity analysis is discussed in section 3.5 (Fig. S3)

To account for the correlations in the data-set we therefore add a second constraint in the source apportionment calculations, based on the relation to the TC concentrations:

$$\begin{pmatrix} f_{C3}(i) \\ f_{fossil}(i) \\ f_{C4}(i) \end{pmatrix} = \frac{1}{[TC(i)]} \cdot \begin{pmatrix} f_{C3,slope} \\ f_{fossil,slope} \\ f_{C4,slope} \end{pmatrix} + \begin{pmatrix} f_{C3,intercept} \\ f_{fossil,intercept} \\ f_{C4,intercept} \end{pmatrix} \quad (3)$$

Where we, instead of fitting a source vector ($f_{C3}$, $f_{fossil}$, $f_{C4}$) for each individual data pair, fit two vectors: a slope and an intercept of the line, to all data points. This clearly holds the advantage of have fewer fitting parameters. We emphasize that the strength of the correlation of the isotope signatures relative to 1/TC is naturally incorporated into this relation, such that lower correlation of $\delta^{13}C$ w.r.t 1/TC impose weaker constraints on the calculated source fractions, compared to $\Delta^{14}C$.

The source fractions were computed using numerical Markov chain Monte Carlo simulations, implemented in Matlab, ver. 2015b, using 1000.000 iterations with a burn-in (initial search phase) of 10.000 and a data thinning of 10 (removing step-wise correlations). The stochastic perturbation parameter was adjusted as to obtain an acceptance ratio of 0.23, which has been suggested to be optimal for Metropolis-Hastings algorithms (Roberts et al., 1997). For this set-up, the variability in the numerically estimated parameters, e.g., the standard deviation of the relative source fraction, is lower than 1% of the mean value, suggesting good convergence (Winiger et al., 2017).

### 2.6 Air Mass Back trajectories and Remote Sensing

10-days air mass back-trajectories (arrival height 2690 m.a.s.l. (100 m.a.g.l.) and 3090 m.a.s.l. (500 m.a.g.l.) were calculated using the NOAA Hybrid Single Particle Lagrangian Integrated Trajectory Model (HYSPLIT) (Figs. 1 and S1). Remote sensing fire-spot detections were retrieved from the NASA Fire Information for Resource Management Services (FIRMS) database, based on retrievals from the Moderate Resolution Imaging Spectroradiometer (MODIS) satellite product.

## 3 Results and Discussion

### 3.1 Back-trajectory analysis

Air mass back-trajectory analysis show that the air masses arriving at the Rwanda Climate Observatory (RCO) during the filter collection periods are overall easterly/southeasterly (Figs. 1 and S1). There is some overlap between the wet and boreal summer dry seasons, but overall there is a seasonal switch, where the wet seasons air masses are more of directly eastern origins (e.g., Uganda and Kenya and Tanzania), whereas the dry are more directly southeastern (e.g., Burundi, Tanzania and Democratic Republic of Congo). During the dry season there are extensive fires to

the south of RCO, mainly to the south-west (DR of Congo and Angola). However, the air masses also pass over regions with comparably high fire activities in the southeast, mainly in Tanzania. Nevertheless, we emphasize that back-trajectory analysis is challenging in mountainous regions (e.g., Winiger et al., 2019), and the actual geographical footprints are expected to be broader, e.g., due to the propagating effects of turbulence. Here we interpret the back-trajectories qualitatively to visualize overall air mass transport patterns.

### 3.2 Concentrations of fine aerosol components

During the present campaign, the $PM_{2.5}$ carbonaceous and inorganic ion components show a strong seasonal variability, with elevated levels during the dry JJA season (Fig. 2, Table S1). The dry/wet season ratios for TC, EC, WSOC, $NO_3^-$, $SO_4^{2-}$, $NH_4^+$ and $K^+$, were 4.2, 7.0, 4.1, 12.6, 3.0, 3.2 and 8.8, respectively (Table 1). This variability suggests differences in the aerosol sources and atmospheric processing, in addition to seasonality in meteorology, e.g., varying boundary layer heights or precipitation. The sea-salt contributions to the ions are overall estimated to be less than 1%, using corrections with sodium ions (Blanchard and Woodcock, 1980). We here report the actual concentrations to facilitate direct comparisons with previous studies (Table 1). Overall, these differences reflect differences in aerosol atmospheric lifetime, air mass transport pathways and emissions seasonality (e.g., fires). Elevated ratios of EC and $K^+$ suggests an increased influence from biomass burning during the dry season. $NO_3^-$, which displays the largest seasonal shift, is often associated with oxidized $NO_x$ from traffic emissions or lightning strikes. However, it is also typically elevated in emissions from savanna fires (Table 1; e.g., Gao et al., 2003; Formenti et al., 2003).

The dry season concentrations of carbonaceous aerosols components and inorganic ions reported here are overall in good agreement with the concentrations observed dry season rural and aged savanna fire air masses (Table 1). The BC values are in the same range as has previously been observed at Mt. Kenya ($0.72 \pm 0.06$ μgC $m^{-3}$, Gatari et al., 2003). During atmospheric aging of a biomass plume, the values of OC, EC and $K^+$ decrease by a factor of 2-3, whereas other components are relatively unaffected (Table 1). However, the effects appear variable, as compared with savanna fires in South Africa (Gao et al., 2003).

RCO is situated not far away from the Nyiargongo and Nyamuragria Volcanoes in eastern Democratic Republic of Congo. High spatial resolution (13x24km$^2$) satellite-monitoring of the $SO_2$ levels show a near-constant emissions from these volcanoes over the time period covering the present campaign, likely affecting the observed sulfate levels (Barrière et al., 2017). Here we observe a spike in sulfate levels (~ 5μg m$^{-3}$) during the week starting of the 13$^{th}$ of June 2015 (Fig. 2), but with no clear linkage to an increase in volcanic $SO_2$ emissions.

### 3.3 Source marker ratios and correlations

Overall, the ratios of different aerosol components provide insights into sources or atmospheric processes. Here, the EC/TC shows a distinct seasonality (Fig. 3 and Table S1). More commonly analyzed, though, is the OC/EC ratio (=(TC-EC)/EC), with elevated levels during the wet season (11±3) compared to the dry season (7±3; Table S1). The OC/EC-ratio is sometimes used as a marker for biomass burning, but is highly influenced by burning conditions such as flaming or smoldering fires. In addition, it is highly influenced by atmospheric processes such as secondary organic aerosol (SOA) formation or photo-chemical aging (e.g., Dasari et al., 2019). The dry season values observed here are similar to what has been observed in background air at other dry season Sub-Saharan African sites (Table 1).

Similarly, the $NH_4^+$/TC and $SO_4^{2-}$/TC are also elevated during the wet seasons (Fig. 3), while decreasing during the dry seasons, suggesting a different source profile compared to EC, $K^+$ and $NO_3^-$, including potential volcanic input of $SO_2$. In contrast, the WSOC/OC-ratio shows no clear seasonality, indicating small differences in sources and atmospheric processing of water-soluble and water-insoluble organic components over the year. TC correlates with $K^+$ ($R^2$ = 0.95, p<0.01) and $NO_3^-$ ($R^2$ = 0.95, p<0.01), suggesting that the incomplete combustion regime during the present campaign is governed by biomass emissions, e.g., savanna burning. Taken together, these ratios qualitatively suggest that the aerosol regime at RCO is strongly influenced by occasional input of biomass burning products during the boreal dry season.

### 3.4 Carbon isotopes

Radiocarbon ($\Delta^{14}C$) and stable-carbon ($\delta^{13}C$) provides detailed information regarding the sources and atmospheric processing of carbonaceous aerosols. Here, we investigated the signatures of TC for roughly every second sample during the campaign. The $\Delta^{14}C$-marker is not influenced by atmospheric processing, and may be used to directly compute the relative contributions of fossil vs biomass/biogenic sources with high precision, Eq. (1). The $\Delta^{14}C$-signature show an oscillation over the seasons, ranging between -84‰ (November, 2014) and +30‰ (July, 2015) (Fig. 4 and Table S1). Thus, during the JJA season, the $\Delta^{14}C$-signature exceed the signature for atmospheric $CO_2$ (+20‰, Graven, 2015; Turnbull, 2017).

Using Equation (1), the percentage biomass/biogenic TC for the $\Delta^{14}C$ = +30‰ sample is 97%. During the wet season, the percentage derived from fossil reaches 13%, possibly of a more local derivation. $\Delta^{14}C$ correlates with 1/TC ($R^2$ = 0.85, $p<0.01$), which suggests that the variability in concentrations can be explained as a two-component mixture: a stable background and a temporally fluctuating source (Keeling, 1958) (Fig. 5A). This inverse relation gives $\Delta^{14}C$ = +37 ± 6‰ as TC approaches infinity, showing that the non-background component is of biogenic/biomass burning origins. The $\Delta^{14}C$ signatures for TC reported here are overall higher than for monitoring sites in South and East Asia (Sheesley et al., 2012; Kirillova et al., 2014; Bikkina et al., 2016).

In contrast to $\Delta^{14}C$, the $\delta^{13}C$-value is influenced by both atmospheric processes (i.e., kinetic isotope effects, KIE) and source signatures. Here, the $\delta^{13}C$-value shows a similar pattern relative to the $\Delta^{14}C$-value, depleted in $^{13}C$ (min $\delta^{13}C$ = -27‰) during wet seasons, and higher during the dry season (max $\delta^{13}C$ = -21 ‰) (Fig. 4B). The correlation w.r.t. 1/TC ($R^2$=0.55, $p<0.1$) is weaker compared to $\Delta^{14}C$ (Fig. 5B). The direct fossil vs biomass source correlation from the $\Delta^{14}C$ Keeling curve is also driving the $\delta^{13}C$-signatures, but the higher variability is explained by larger endmember variability and potential influence of KIE, see Section 3.5. An overall enrichment in $^{13}C$ has been found in aged air masses in South Asia, especially for WSOC (Kirillova et al., 2013; Dasari et al., 2019), but less so for TC. In fact, the enrichment of $^{13}C$ in WSOC often appears to be counter-acted by a decrease in water-insoluble OC (e.g., Yan et al., 2017; Fang et al., 2017).

The TC $\delta^{13}C$ values, and their seasonal trend, are similar to what has previously observed in fine aerosols at a rural site in Tanzania (May – August, 2011, Mkoma, et al., 2014). However, the

temporal trend appears shifted in the RCO samples from values around -25 ‰ to around 22 ‰ in mid-May. At the Tanzanian site, a similar shift occurs in mid-June. In addition to the complications of comparing measurements conducted at different sites during different years, there is a good agreement in the $\delta^{13}C$-values, and the temporal offset may be explained by inter-tropical convergence zone position variability. Similarly, the $\delta^{13}C$-value for TC at a savanna woodland site in Zambia, observed during August-September 2000, was -21.8±0.8 ‰ (Billmark et al., 2003), while values between -19.3 and –23.6 ‰ were observed at sites in the Ivory Coast (Cachier et al., 1985).

### 3.5. Carbon isotope-based source apportionment

By combining the $\Delta^{14}C$ and the $\delta^{13}C$-values we can by isotopic mass balance resolve three major sources of TC at the RCO, Eq. (2). However, there are some important considerations to this approach: First, the $\delta^{13}C$-value is not an exclusive source marker, but is also affected by atmospheric processing (e.g., photo-chemical oxidation and secondary formation). Second, the main source categories must be defined and distinguishable using carbon isotopes. Third, the source-values of the isotope-signatures, the endmembers, and their natural variability need to be established.

As mentioned, the $\delta^{13}C$-value of bulk TC appears to be considerably less affected by atmospheric processing compared to sub-components, such as WSOC. Here, the temporal variation of the $\delta^{13}C$-value is qualitatively similar to that of $\Delta^{14}C$-value (Fig. 4). Since $\Delta^{14}C$ is not affected by atmospheric reactions, this suggests that source variability is a key driver of the $\delta^{13}C$ variability. Furthermore, the WSOC/OC is virtually constant throughout the year (Fig. 3); the WSOC/OC has been found to be highly affected by atmospheric processing and related to shifting $\delta^{13}C$ (Kirillova et al., 2013; Yan et al., 2017; Fang et al., 2018; Dasari, 2019). Here, we therefore assume that the $\delta^{13}C$-ratio of TC is not strongly perturbed by atmospheric processing during long-range transport, and may thus be used as a source marker. Nevertheless, we explore the potential influence on KIE, as well as endmember variability, on the source apportionment results in a sensitivity analysis.

Turning to potential sources, there is a multitude of potential source categories for TC in SSA. However, many of these fall in broad categories, with similar carbon isotope signatures. Around the world, the applications of dual carbon isotope source apportionment techniques in ambient TC

mainly identified/considered 6 broad source categories: $C_3$ plants, $C_4$ plants, liquid fossil fuels (e.g., traffic), coal combustion (solid fossil), gas flaring (gaseous fossil) and marine emissions (Winiger et al., 2019; Andersson et al., 2015; Kirillova et al., 2013). Overall, the practice of coal combustion in SSA is expected to be much less frequent than in, for example, South and East Asia, and we therefore do not consider this source further. In addition, marine emissions are not expected to have a large influence at RCO, supported by the low estimates of marine contributions to the inorganic ions (<1%). For gas flaring, there are potential distant sources around the Arabian Peninsula and off the west coast of Africa, in the Gulf of Guinea. However, given the distances to the RCO station and the prevailing wind directions, emissions from flaring are not expected to affect the site, while the $\delta^{13}C$-signatures for gas-flaring are strongly depleted in $^{13}C$ ($\delta^{13}C$<-38‰; Winiger et al., 2017) and even a small contribution would shift the observed values significantly.

The remaining three main source categories are the two biomass sources of $C_3$ (e.g., trees) and $C_4$ plants (e.g., sugarcane and certain grasses) and liquid fossil fuels (Fig. 6). Aerosols from liquid fossil fuel sources have a $\Delta^{14}C_{fossil}$ = -1000‰ (completely depleted in $^{14}C$) and a $\delta^{13}C_{fossil}$ = -25.5±1.3‰ (Widory, 2006; Andersson et al., 2015). The $\Delta^{14}C$ of biomass was established in Section 2.4 as $\Delta^{14}C_{C3} = \Delta^{14}C_{C4}$ = +57 ± 52‰. The $\delta^{13}C$ of $C_3$-plants in general is -27.1±2‰ (Bender, 1971; O'Leary, 1988). However, for aerosols generated from $C_3$-plants this value may be either enriched (e.g., ~ 0.5‰ biomass burning) or depleted (e.g., ~ 0 to 4‰ during SOA formation) (Turekian, 1998; Das et al. 2010, Mkoma et al., 2014; Aguilera and Whigham, 2018). In any case, the numerical spread in the $\delta^{13}C$-value of these different sources are largely overlapping with that of the raw materials, and we therefore use this value here. The $\delta^{13}C$ of $C_4$-plant materials is -13.1±1.2‰ (Bender, 1971; O'Leary, 1988; Turekian 1998). However, during incomplete combustion, the $\delta^{13}C_{C4}$ may be reduced by a factor ranging from 0 to 7‰, largely dependent on burning conditions and species (Martinelli, 2002; Das et al., 2010; Aguilera and Whigham, 2018). Accounting for such effects in source apportionment is a challenge, especially since the reported values are ranges and not mean and variability, and thus are highly influenced by potential outliers. We here use a method discussed in Andersson et al. (2015) to address the issue of statistical analysis of ranges by assuming that the total range corresponds to the 95% confidence intervals of a normal distribution. This corresponds to the range of 4 times the standard deviation, yielding $\sigma$ = 7/4‰, while the mean is -7/2‰. Combining this with the variability of the of pure $C_4$-plants we

obtain: $\delta^{13}C_{C4}$: -16.6 ± 2.2‰, where $\sigma^2 = 1.2^2 + (7/4)^2$ ‰$^2$. These values are also what is obtained by numerical estimation of the convolution of a normal distribution ($\mu$ = -16.6, $\sigma$ = 1.2‰) with a uniform distribution ([-7, 0] ‰), adding to the strength of statistical representation.

The fractional source contributions of fossil fuel, $C_3$ and $C_4$ to TC are computed with Eqs. (2) and (3) (Fig. 7). It is well-established that accurate estimation of the fractional source contributions requires explicit incorporation of the endmember variability, and we here use a Bayesian framework driven by Markov chain Monte Carlo simulations for this purpose (Andersson, 2011; Andersson et al., 2015). To estimate the influence of the intra-endmember mixing during atmospheric transport we use the correlations of the isotopes with TC within the Bayesian framework, see section 2.5, to account for the endmember averaging during atmospheric transport (Martens et al., 2019) (Fig. 5). The resulting fractional contributions display a large variability when comparing wet and dry conditions (Fig. 7A and Table S2). The dry season is characterized by relatively higher $C_4$-plant contributions, whereas the relative contributions of fossil fuels and $C_3$-plants increase during the wet seasons. Back-calculating the isotope signatures from the computed source fractions from the MCMC-simulations essentially reproduce the Keeling relations relative to 1/TC (Figs. 5 and S2). To check influence of the number of data points used in the Keeling-based MCMC, we computed comparative scenarios where every third data point was used (starting at data point 1, 2 and 3 respectively) (Fig S3). The standard deviations for the calculated $f_{C3}$ are on average doubled when only every third point are used (5% vs 10%), showing how correlations between multiple data points aids in constraining the sources.

Since the $\delta^{13}C$ endmembers for, in particularly $C_4$-plants, are not well-constrained, we also employed a sensitivity analysis w.r.t. endmembers and the potential influence of KIE (Tables S2 – S5 and Figs. S4 – S6). In addition to the above discussed best estimate scenario, we tested two $\delta^{13}C_{C4}$ scenarios: a 'minimum KIE scenario' with zero KIE ($\delta^{13}C_{C4}$ -13.1±1.2‰) and a 'maximum KIE scenario', with a depletion by 5.9‰ ($\delta^{13}C_{C4}$ -19.0±2.2‰). The maximum KIE scenario was established such as the $f_{C4}/(f_{C4}+f_{C3})$-ratio would be 62% as TC approach infinity, and thus 100% savanna contributions, see Eq. (4). As expected, these scenarios significantly shift the estimated relative $C_4$ contributions, resulting in a total range of the sample period averages of 24% (min-KIE; min 6% max 32%) to 42% (max-KIE; min 10%, max 58%), thus providing lower and upper bounds (Figs. S4 and S5 and Tables S3 and S4). The corresponding value for our best estimate is

32% (max 44%, min 8%). In addition, we investigated a scenario with a 3‰ depletion of the fossil endmember ($\delta^{13}C_{fossil}$ -28.5±1.3‰). Since the fossil contribution is overall low as determined by $\Delta^{14}C$, and since $\Delta^{14}C$ constrains the fossil contribution independently of the $\delta^{13}C$ data, this shift has no significant influence on the computed source fractions 6% (max 11%, min 3%) (Fig. S6 and Table S5). Overall, we stress that these three sensitivity test scenarios represent extreme limits, and the a priori least biased scenario is the initially outlined best scenario.

By combining the estimated fractional source contributions with the TC concentrations, we can estimate the concentrations from the different sources (Fig. 7B), revealing a more accentuated source variability. The average dry-to-wet ratios of the TC to $C_3$-plants, $C_4$-plants and fossil fuels are 3, 5 and 2, respectively.

Savannas are the main biome supporting $C_4$-plants in SSA. For East African savannas, $\delta^{13}C$ data suggests that ~ 62% ($f_{C4,NPP}$) of the net primary production (NPP) is from $C_4$-plants (the rest mainly $C_3$-plants, Lloyd et al., 2008). Thus, one may assume that the source characteristics of TC emitted from savanna burning should represent this plant-signature distribution. However, the aerosol emissions modulate the NPP activity through emission factors (EF). The uncertainties of EFs from different biomass burning activities are generally large and overlapping (Andreae, 2019). As a first approximation, we here use $f_{C4,NPP}$ to estimate the fractional contribution of savanna emissions to TC ($f_{savanna}$) as (i = sample index):

$$f_{savanna}(i) = \frac{f_{C4}(i)}{f_{C4,NPP}} \quad (4)$$

This analysis shows that the dry season carbonaceous aerosol regime is dominated by savanna fire emissions reaching up to 71% (Fig. 7 and Table S2). These results agree with the elevated levels of EC, $K^+$ and $NO_3^-$ during the dry season (Table S1).

## 5. Outlook

In this paper we find that the aerosol composition of the emissions affecting the Rwanda Climate Observatory (RCO) may be described as a two-state source mixture: a regional/local background signal modulated by savanna fire emissions. Multiple studies have shown that savanna fires strongly influence the aerosol regime in SSA. Here, we estimate the savanna fire contributions for

carbonaceous aerosols to range from 13% (wet season; $TC_{savanna}$ = 0.2 μg $m^{-3}$) to 71% (dry season; $TC_{savanna}$ = 9.7 μg $m^{-3}$) at RCO (Fig. 7). The savanna fires are believed to be mainly lit by humans, and although these activities have been ongoing perhaps throughout the Holocene, these anthropogenic activities strongly perturb the regional ecosystems, climate and air quality (e.g., Bird and Cali, 1998; Archibald et al., 1998). The annual SSA savanna carbon budget represents a net $CO_2$ source to the atmosphere (Williams, 2007; Cais et al., 2011; Valentini et al., 2014; Palmer et al., 2019). Finding more sustainable alternatives to the slash-and-burn practices in SSA could therefore possibly turn the region into a carbon sink. For instance, implementation of early dry season burning may be a possible strategy (Lipset-Moore et al., 2018). Savanna fire mitigation would also improve the regional air quality and stabilize precipitation patterns (Hodnebrog et al., 2015; Heft-Neal et al., 2018; Bauer et al., 2019).

Nevertheless, the current level of scientific understanding of the impact of savanna burning on the environmental system is poor, as are the couplings/responses to climate change, population growth, urbanization and other key socio-economic and environmental challenges for sustainable development in SSA (e.g., IPCC, 2014; Liousse et al., 2015; Brandt et al., 2017; UNDP, 2018). Savanna burning mitigation, or shifts in in fire regime due to climate change, may change the present steady-state in unpredictable ways (e.g., Abreu et al., 2017). To better constrain the multiple environmental impacts of savanna burning in SSA, the comparably few ongoing ground-based in situ observations should be expanded and solidified (Williams, 2007; Cais et al., 2011; Kulmala, 2018; López-Ballesteros et a., 2018). For instance, observations of source-segregated aerosol concentrations provides multiple opportunities for advancing our knowledge of environmental processes relevant to SSA, including providing means for testing chemical-transport models; examining the relative importance of cooling vs warming (e.g., BC) aerosols; ground-truthing remote sensing products and detailed monitoring of the expected rapid change over the coming decades, including the effects of climate warming, population growth and urbanization.

*Data availability:* The chemical and isotopic data, as well as the MCMC-derived relative source contributions of $C_3$-plants, $C_4$-plants and fossil, and the corresponding source-segregated TC concentrations is provided in the supplementary information.

*Competing interests:* The authors declare that they have no conflict of interest.

*Author contributions*: AA wrote the manuscript, set-up the $PM_{2.5}$ high-volume sampler at RCO, and analyzed the data. ENK and SD conducted the carbonaceous aerosol quantifications and isolations for isotopes, and IC analysis. JG worked with the instruments, including helping or leading installation, and provided feedback on data analysis. KEP was instrumental in setting up the RCO and did most of the initial instrument installation. HLD served as the RCO station chief scientist for three years. JN and JdDN worked as technical coordinators of the project at different times and facilitated the operations of the station as well as providing feedback on analysis. BS was our University of Rwanda liaison as the head of the Master's program in atmospheric and climate science. RGP is the head of the AGAGE network and is the MIT liaison to the RCO, and was essential in the setup of the observatory and scientific analysis. All authors commented on the manuscript.

*Acknowledgement*s. We thank the generous MIT alumni donors to the MIT-Rwanda Climate Observatory Project and the MIT Center for Global Change Science. We also thank the Government of Rwanda and the Rwanda Ministry of Education. We also wish to acknowledge the essential contributions of the Mugogo station technical experts Theobard Habineza, Modeste Mugabo, Olivier Shyaka, and Gaston Munyampundu and RBA technician Yves Fidele, without which running this station would be impossible. AA acknowledges project grants from the Swedish Research council (projects 348-2013-114 and 2017-05687). ENK acknowledges the People Programme (Marie Curie Actions) of the European Union's Seventh Framework Programme (FP7/2007-2013) under REA grant agreement 623386. We acknowledge the use of data and imagery from LANCE FIRMS operated by NASA's Earth Science Data and Information System (ESDIS) with funding provided by NASA Headquarters. The authors gratefully acknowledge the NOAA Air Resources Laboratory (ARL) for the provision of the HYSPLIT transport and dispersion model and/or READY website (http://www.ready.noaa.gov) used in this publication.

## References


Abreu, R.C., Hoffmann, W.A., Vasconcelos, H.L., Pilo, N.A., Rossatto, D.R., Durigan, G.: The biodiversity cost of carbon sequestration in tropical savanna. Sci. Advan. 3, doi: 10.1126/sciadv.1701284, 2017.

Aguilera, J., Whigham, L.D.: Using the $^{13}C/^{12}C$ carbon isotope ratio to characterize the emission sources of airborne particulate matter: a review of literature. Isotopes Environ. Health. Stud 54, 573-587, doi: 10.1080/10256016.2018.1531854, 2018.

Andersson, A.: A systematic examination of a random sampling strategy for source apportionment calculations. Sci. Tot. Environ. 412-413, 232-238, doi: 10.1016/j.scitotenv.2011.031, 2011.

Andersson, A., Deng, J., Du, K., Zheng, M., Yan, C., Sköld, M., Gustafsson, Ö.: Regionally-varying combustion sources of the January 2013 severe haze events over Eastern China. Environ. Sci. Technol. 49, 2038-2043, doi: 10.1021/es503855e, 2015.

Andreae, M.O.: Emission of trace gases and aerosols from biomass burning – An updated assessment. Atmos. Chem. Phys. Discuss. doi: 10.5194/acp-2019-303, 2019.

Archibald, S., Staver, A.C., Levin, S.A.: Evolution of human-driven fire regimes in Africa. Proc. Nat. Acad. Sci. 109, 847-852, doi: 10.1073/pnas.1118648109, 2012.

Aurela, M., Beukes, J.P., van Zyl, P., Vakkari, V., Teinilä, K., Saarikoski, S., Laakso, L.: The composition of ambient and fresh biomass: burning aerosols at a savannah site, South Africa. South Afr. J. Sci. 112, 1-8, doi: 10.17159/ sajs.2016/20150223, 2016.

Barrière, J., Oth, A., Theys, N., d'Oreye, N., Kervyn, F.: Long-term monitoring of long-period seismicity and space-based $SO_2$ observation at African lava lake volcanoes Nyiarango and Nyamulagira (DR Congo). Grophys. Res. Let. 44, 6020-6029, doi: 10.1002/2017GL073348, 2017.

Bauer, S.E., Im, U., Mezuman, K., Gao, C.Y.: Desert dust, industrialization, and agricultural fires: health impacts of outdoor air pollution in Africa. J. Geophys. Res. 124, 4104-4120, doi: 10.1029/2018JD029336, 2019.

Bender, M.M.: Variations in the $^{13}C/^{12}C$ ratios of plants in relation to the pathway of photosynthetic carbon dioxide fixation. Phytochem. 10, 1239-1244, doi: 10.1016.S0031-9422(00)84324-1, 1971.

Bikkina, S., Andersson, A., Sarin, M.M., Sheesley, R.J., Kirillova, E., Rengarajan, R., Sudheer, A.K., Ram, K., Gustafsson, Ö.: Dual isotope characterization of total organic carbon in wintertime carbonaceous aerosols for northern India. J. Geophys. Res. 121, doi: 10.1002/2016JD024880, 2016.

Billmark, K.A., Swap, R.A., Macko, S.A.: Stable isotope and GC/MS characterization African aerosols. South African J. Sci. 101, 177-170, 2005.

Birch, M.E., Cary, R.A.: Elemental carbon-based method for monitoring occupational exposures to particulate diesel exhaust. Aerosol Sci. Technol 25, doi: 10.1080/02786829608965393, 1996.

Bird, M.I., Cali, J.A.: A million-year record of fire in sub-Saharan Africa. Nature 394, 767-769, doi: 10.1038/29507, 1998.

Blanchard, D.C., Woodcock, A. H.: The production, concentration, and vertical distribution of the sea-salt aerosol. Annal. N.Y. Acad. Sci. doi: 10.1111/j.1749-6632.1980.tb17130.x, 1980.

Bond, T.C., Doherty, S.J., Fahey, D.W., Forster, P.M., Berntsen, T., DeAngelo, B.J., Flanner, M.G., Ghan, S., Kärcher, B., Koch, D., Kinne, S., Kondo, Y., Quinn, P.K., Sarofim, M.C., Schultz, M.G., Schultz, M., Venkataram, C., Zhang, H., Zhang, S., Bellouin, N., Guttikunda, S.K., Hopke, P.K., Jacbonson, M.Z., Kaiser, J.W., Klimont, Z., Lohmann, U., Schwarz, J.P., Shindell, D., Storelvmo, T., Warren, S.G., Zender, C.S.: Bounding the role of black carbon in the climate system: A systematic assessment. J. Geophys. Res. 118, 5380-5552, doi: 10.1002./jgrd.50171, 2013.

Brandt, M., Rasmussen, K., Penuelas, Tian, F., J., Schurgers, G., Verger, A., Mertz, O., Palerm, J.R.B., Fensholt, R.: Human population growth offsets climate-driven increase in woody vegetation in sub-Saharan Africa. Nature Ecol. Evol. 1, doi: 10.1038/s41559-017-0081, 2017.

Brito, J., Freney, E., Dominutti, P., Borbon, A., Haslett, S.L., Batenburg, A.M., Colomb, A., Dupuy, R., Denjean, C., Burnet, F., Bourriane, T., Deroubaix, A., Sellegri, K., Borrmann, S. Coe,

H., Flamant, C., Knippertz, P., Schwarzenboeck, A.: Assessing the role of anthropogenic and biogenic source on PM1 over southern West Africa using aircraft measurements. Atmos. Chem. Phys. 18, 757-772, doi: 10.5194/acp-18-757-2018, 2018.

Cachier, H., Buat-Menard, P., Fontuge, M., Ranhcer, J.: Source terms and source strengths of the carbonaceous aerosol in the tropics. J. Atmos. Chem. 3, 469-489, doi: 10.1007/BF00053872, 1985.

Cahoon, D.R., Stocks, B.J., Levine, J.S., Cofer III, W.R., O'Neil, K.P.: Seasonal distribution of African savanna fires. Nature, 359, 812-815, doi: 10.1038/359812a0 , 1992.

Cais, P., Bombelli, A., Williams, M., Piao, S.L., Chave, J., Ryan, C.M., Henry, M., Brender, P., Valentini, R.: The carbon balance of Africa: synthesis of recent research studies. Phil. Trans. Roy. Soc. A 369, 2038-2057, doi: 10.1098/rsta.2010.0328, 2011.

Das, O., Wang, Y., Hsieh, Y.-P.: Chemical and carbon isotopic characteristics of ash and smoke derived from burning of C3 and C4 grasses. Org. Geochem. 41, 263-269, 10.1016/j.orggeochem.2009.11.001, 2010.

Dasari, S., Andersson, A., Bikkina, S., Holmstrand, H., Budhavant, K., Sateesh, S., Asmi, E., Kesti, J., Backman, J., Salam, A., Singh Bisht, D., Tiwari, S., Hameed, S., Gustafsson, Ö.: Photochemical degradation affects the light absorption of water-soluble brown carbon in the South Asian outflow. Sci. Adv. 5, doi: 10.1126/sciadv.aau8066, 2019.

DeWitt, H.L., Gasore, J., Rupakheti, M., Potter, K.E., Prinn, R.G., Ndikubwimana, JdD., Nkusi, J., Safari, B.: Seasonal and diurnal variability in O3, black carbon, and CO measured at the Rwanda Climate Observatory. Atmos. Chem. Phys, 19, 2063-2078, doi: 10.5194/acp-19-2063-201, 2019.

Fang, W., Andersson, A., Zheng, M., Lee, M., Holmstrand, H., Kim, S-W., Du, K., Gustafsson, Ö.: Divergent evolution of carbonaceous aerosols during dispersal of East Asian haze. Sc. Rep. 7, doi: 10.1038/s41598-017-10766-4, 2017.

Formenti, P., Elbert, W., Maenhaut, W., Haywood, J., Osborne, S., Andreae, M.O.: Inorganic and carbonaceous aerosols during the Southern African Regional Science Initiative (SAFARI 2000)

experiment: Chemical characteristics, physical properties, and emission data for smoke from African biomass burning. J. Geophys. Res. 108. Doie: 10.1029/2002JD002408, 2003.

Gao, S., Hegg, D.A., Hobbs, P.V., Kirchstetter, T.W., Magi, B.I., Sadilek, M.: Water-soluble organic components in aerosols associated with savanna fires in southern Africa: Identification, evolution and distribution. J. Geophys. Res. 108, doi: 10.1029/2002JD002324, 2003.

Gatari, M.J., Boman, J.: Black carbon and total carbon measurements at urban and ruralt sites in Kenya, East Africa. Atmos. Environ. 8, 1149-1154, doi: 10.1016/S1352-2310(02)01001-4, 2003.

Graven, H.: Impact of fossil fuel emissions on atmospheric radiocarbon and various applications of radiocarbon over this century. Proc. Nat. Acad. Sci. 112, 9542-9545, doi: 10.1073/pnas.1504467112, 2015.

Gustafsson, Ö., Kruså, M., Zencak, Z., Sheesley, R.J., Granat, L., Engström, E., Praveen, P.S., Rao, P.S.P., Leck, C., Rodhe, H.: Brown clouds over South Asia: Biomass or fossil fuel combustion? Science 323, 495-498, doi: 10.1126/science.1164857, 2009.

Heft-Neal, S., Burney, J., Bendavid, E., Burke, M.: Robust relationship between air quality and infant mortality in Africa. Nature 559, 254-258, doi: 10.1038/s41586-018-0263-3, 2018.

Hodnebrog, Ø., Myhre, G., Forster, P.M., Sillman, J., Samset, B.H.: Local biomass burning is a dominant cause of the observed precipitation reduction in southern Africa. Nature Com. 7, doi: 10.1038/ncomms11236, 2015.

IPCC – Inter-Governmental Panel for Climate Change: AR5 Climate Change 2013: The physical science basis. ISBN 978-1107661820, 2013.

IPCC – Inter-Governmental Panel for Climate Change: AR5 Climate Change 2014: Impacts, adaptation and vulnerability. ISBN 978-1-107-68386-0, 2014.

Keeling, C.D.: The concentration and isotopic abundances of atmospheric carbon dioxide in rural areas. Geochem. Cosmochim. Acta. 13, 322-334, doi: 10.1016/0016-7037(58)90033-4, 1958.

Kirchstetter, T.W., Novakov, T., Hobbes, P.V., Magi, B.: Airborne measurements of carbonaceous aerosols in southern Africa during the dry biomass season. J. Geophys. Res. 108. Doi: 10.1029/2002JD002171, 2003.

596 Kirillova, E.N., Andersson, A., Sheesley, R.J., Kruså, M., Praveen, P.S., Budhavant, K., Safai,
597 P.D., Rao, P.S.P., Gustafsson Ö: $^{13}C$ and $^{14}C$-based study of sources and atmospheric processing
598 of water-soluble organic carbon (WSOC) in South Asian aerosols. J. Geophys. Res. 118, 621-626,
599 doi: 10.1002/jgrd.50130, 2013.

600 Kirillova, E.N., Andersson, A., Han, J., Lee, M., Gustafsson, Ö.: Sources and light absorption of
601 water-soluble organic carbon aerosols in the outflow from northern China. Atmos. Chem. Phys.
602 14, 1413-1422, doi: 10.5194/acp-14-1413-2014, 2014.

603 Kulmala, M.: Build a global Earth Observatory. Nature 553, 21-23, 2018.

604 Liousse, C., Assamoi, E., Criqui, C., Rosset, R.: Explosive growth in African combustion
605 emissions from 2005 to 2030. Environ. Res. Lett. 9, doi: 10.1088/1748-9326/9/3/035003, 2014.

606 Lipset-Moore, G.J., Wolff, N., Game, E.T.: Emissions mitigation opportunities for savanna
607 countries from early dry season fire management. Nature Com. 9, doi: 10.1038/s41467-018-
608 04687-7, 2018.

609 Lloyd, J., Bird, M.I., Vellen, L., Miranda, A.C., Veenendaal, E.M., Djagbletey, G., Miranda, H.S.,
610 Cook, G., Faruqhar, G.D.: Contributions of woody and herbacoues vegetation to tropical savanna
611 ecosystem productivity: a quasi-global estimate. Tree Phys. 28, 451-468, doi:
612 10.1093/treephys/28.3.45, 2008.

613 López-Ballesteros, A:, Beck, J., Bombelli, A., Grieco, E., Lorenkova, E.K., Merbold, L.,
614 Brümmer, C:, Hugo, W., Scholes, R., Vackar, D., Vermeulen, A., Acosta, M., Butterbach-Bahl,
615 K., Helmschrot, J., Kim, D.-G., Jones, M., Jorch, V., Pavleka, M., Skjelvan,I., Saunders, M.:
616 Towards a feasible and representative pan-African research infrastructure network for GHG
617 observations. Environ. Res. Lett. 13, doi: 10.1088/1748-9326/aad66c, 2018.

618 Maenhaut, W., Salma, I., Cafmeyer, J., Annegarn, H.J., Andreae, M.O.: Regional atmospheric
619 aerosols composition and sources in the eastern Transvaal, South Africa, and impact of biomass
620 burning. J. Geophys. Res. 101, 23631-23650, 1996.

621 **Martens, J., Wild, B., Pearce, C., Tesi. T., Andersson, A., Bröder, L., O'Regan, M.,**
622 **Jakonsson, M., Sköld, M., Gemery, L., Cronin, T.M., Semiletov, I., Dudarev, O.V.,**
623 **Gustafsson, Ö.: (2019) Remobilization of Old Permafrost Carbon to Chukchi Sea Sediments**

**During the End of the Last Deglaciation. Glob. Biogeochem. Cyc. 33, 2-14, doi: 10.1029/2018GB005969**.Martinelli, L.A., Camargo, P.B., Lara, L.B.L.S., Victoria, R.L., Artaxo, P.: Stable carbon and nitrogen isotopic composition of bulk aerosol particles in a C4 plant landscape of southeast Brazil. Atmos. Environ. 36, 2427-2432, doi: 10.1016/S1352-2310(01)00454-X, 2002.

Marwick, T.R., Tamooh, F., Teofuru, C.R., Borget, A.V:, Darchambeau, F., Bouillon, S.: The age of river-transported carbon: global perspective. Glob. Biogeochem. Cyc. 29, 122-137, doi: 10.1002/2014GB004911, 2015.

Mkoma, S.L., Kawamura, K., Tachibana, E., Fu, P.: Stable carbon and nitrogen isotopic compositions of tropical atmospheric aerosols: sources and contribution from burning of $C_3$ and $C_4$ plants to organic aerosols. Tellus B, 66, 1-12, doi: 10.3402/tellusb.v66.20176, 2014.¨

O'Leary, M.H.: Carbon isotopes in photosynthesis. Bioscience 38, 328–36, doi: 10.2307/1310735, 1988.

Palmer, P.I., Feng, L., Chevallier, F., Bösch, H., Somkuti, P.: Net carbon emissions from African biosphere dominate pan-tropical atmospheric $CO_2$ signal. Nature Com. 10. doi: 10.1038/s41467-019-11097-w, 2019.

Puxbaum, H., Rendl, J., Allabashi, R., Otter, L., Scholes, M.C.: Mass balance of the atmospheric aerosol in a South African savanna (Nylsvley, May 1997). J. Geophys. Res. 105, 20697-20706, 2000.

Roberts, G.O., Gelman, A., Gilks, W.R.: (1997) Weak convergence and optimal scaling of random walk Metropolis algorithms. Ann. Appl. Prob. 7, 110-120.Sheesley, R.J., Kirllova, E.N., Andersson, A., Kruså, M., Praveen, P.S., Budhavant, K., Safai, P.D., Rao, P.S.P., Gustafsson, Ö.: Year-round radiocarbon-based source apportionment of carbonaceous aerosols at two background sites in South Asia. J. Geophys. Res. 117, doi: 10.1029/2011JD017161, 2012.

Sinha, P., Hobbs, P.V., Yokelson, R.J., Bertschi, I.T., Blake, D.R., Simpson, I.J., Gao, S., Kirchstetter, T.W., Novakov, T.: Emissions of trace gases and particles from savanna fires in southern Africa. J. Geophys. Res. 108, doi: 10.1029/2002JD002325, 2003.

651 Swap, R.J., Annegard, H.J., Suttles, J.T., King, M.D., Platnick, S., Privette, J.L., Scholes, R.J.:
652 Africa burning: A thematic analysis of the Southern African regional science initiative (SAFARI
653 2000). J. Geophys. Res. 108, doi: 10.1029/2003JD003747, 2003.

654 Tiitta, P., Vakkari, V., Croteau, P., Beukes, J.P., van Zyl, P.G., Josipovic, M., Venter, A.D., Jaaros,
655 K., Pienaar, J.J., Ng, N.L., Canagaratna, M.R:, Jayne, J.T., Kerminen, V.-K., Kokola, H., Kulmala,
656 M., Laaksonen, A., Worsnop, D.R., Laakso, L.: Chemical composition, main sources and temporal
657 variability of PM1 aerosols in southern African grassland. Atmos. Chem. Phys. 14, 1909-1927,
658 doi: 10.5194/acp-14-1909-2014, 2014.

659 Turekian, V. C., Macko, S., Swap, R. J. and Garstang, M.: Causes of bulk carbon and nitrogen
660 isotopic fractionations in the products of vegetation burns: laboratory studies. Chem. Geol. 152,
661 181-192, 10.1016/S0009-2541(98)00105-3, 1998.

662 Turnbull, J.C., Mikaloff Fletcher, S.E., Ansell, I., Brailsford, G.W., Moss, R.C., Norris, M.W.,
663 Steinkamp, K.: Sixty years of radiocarbon dioxide measurements at Wellington, New Zealand:
664 1965-2014. Atmos. Chem. Phys. 17, 14771-14784, doi: 10.5194/acp-17-14771-2017, 2017.

665 UNDP – United Nations Development Programme: 2018 Africa Sustainable Development Report:
666 Towards a transformed and resilient continent. ISBN: 978-92-1-125134-0, 2018.

667 UNEP/WMO – United Nations Environment Programme/World Meteorological Organization:
668 Integrated assessment of black carbon and tropospheric ozone. ISBN: 978-92-807-3142-2, 2012.

669 Valentini, R., Arneth, A., Bombelli, A., Castaldi, S., Cazzolla Gatti, R., Chevallier, F., Cias, P.,
670 Grieco, E., Hartmann, J., Henry, M., Houghton, R.A., Jung, M., Kutsch, W.L., Malhi, Y.,
671 Mayorga, E., Merbold, L., Murray-Tortarolo, G., Papale, D., Peylin, P., Poulter, B:, Raymond,
672 P.A., Santini, M., Sitch, S., Vaglio Laurin, G., van der Werf, G.R., Williams, C.A., Scholes, R.J.:
673 A full greenhouse gases budget of Africa: synthesis, uncertainties, and vulnerabilities.
674 Biogeosciences 11, 381-407, doi: 10.5194/bg-11-381-2014, 2014.

675 WHO – World Health Organization: Health effects of black carbon. ISBN: 978 92 890 0265 3,
676 2012.

677 WHO – World Health Organization: Ambient air pollution: A global assessment of exposure and
678 burden of disease. ISBN: 9789241511353, 2016.

679 Widory, D.: Combustibles, fuels and their combustion products: A view through carbon isotopes.
680 Combust. Theory Mod. 10, 831-841, doi: 10.1080/13647830600720264, 2006.

681 Wild, B., Andersson, A., Bröder, L., Vonk, J:, Hugelius, G., McClelland, J.W., Song, W.,
682 Raymond, P.A., Gustafsson, Ö.: Rivers across the Siberian Arctic unearth the patterns of carbon
683 release from thawing permafrost. Proc. Nat. Acad. 116, 10280-10285, doi:
684 10.1073/pnas.181179116, 2019.

685 Williams, C.A., Hanan, N.P., Neff, J.C., Scholes, R.J., Berry, J.A., Denning, S.A., Baker, D.F.:
686 Africa and the global carbon cycle. Carbon Bal. Manag. 2, 1-13, doi: 10.1186/1750-0680-2-3,
687 2007.

688 **Winiger, P., Andersson, A., Eckhardt, S., Stohl, A., Semiletov, I.P., Dudarev, O.V., Charkin,**
689 **A., Shakova, N., Klimont, Z., Heyes, C., Gustafsson, Ö.: (2017) Siberian Arctic black carbon**
690 **sources constrained by model and observation. Proc. Nat. Acad. Sci. doi:**
691 **10.1073/pnas.1613401114.**Winiger, P., Barrett, T.E., Sheesley, R.J:, Huang, L., Sharma, S.,
692 Barrie, L.A., Yttri, K.E., Evangeliou, N., Eckhardt, S., Stohl, A., Klimont, Z., Heyes, C.,
693 Semiletov, I.P., Dudarev, O.V., Charkin, A., Shakhova, N., Holmstrand, H., Andersson, A.,
694 Gustafsson, Ö.: Source apportionment of circum-Arctic atmospheric black carbon from isotopes
695 and modelling. Sci. Adv. 5, doi: 10.1126/sciadv.aau8052, 2019.

696 Yan, C., Zheng, M., Bosch, C., Andersson, A., Desyaterik, Y., Sullivan, A.P., Collett, J.L., Zhao,
697 B., Wang, S., He, K., Gustafsson, Ö.: Important fossil source contribution to brown carbon in
698 Beijing during Winter. Sci. Rep. 7, doi: 10.1038/srep43182, 2017.

## TABLES

**Table 1.** Concentrations of carbonaceous aerosol (μgC $m^{-3}$) and inorganic ions (μg $m^{-3}$) in fine aerosols from ground-based and airborne measurements over Sub-Saharan Africa (bkg = background).

| Sampling site | TC | OC | BC/EC | WSOC | $NO_3^-$ | $SO_4^{2-}$ | $NH_4^+$ | $K^+$ |
|---|---|---|---|---|---|---|---|---|
| RCO, dry[a] | 9.5±3.7 | 8.2±3.2 | 1.3±0.6 | 5.7±2.1 | 1.2±0.7 | 2.1±1.0 | 0.8±0.3 | 0.7±0.3 |
| RCO, wet[a] | 2.4±1.2 | 2.2±1.1 | 0.20±0.1 | 1.5±0.7 | 0.1±0.1 | 0.7±0.3 | 0.3±0.1 | 0.08±0.05 |
| Rural Tanzania, dry[b] | 7±2 | 6±2 | 1.0±0.3 | 4±1 | 0.18±0.06 | 0.2±0.1 | 0.9±0.7 | 1.5±0.7 |
| Rural Tanzania, wet[b] | 4±1 | 4±1 | 0.5±1.3 | 3±1 | 0.06±0.03 | 0.1±0.1 | 0.2±0.1 | 0.4±0.2 |
| Aircraft, Southern Africa, smoke[c] | N/A | N/A | N/A | N/A | 4.84±0.02 | 10.4±0.6 | N/A | 13.1±0.1 |
| Aircraft, Southern Africa, bkg[c] | N/A | N/A | N/A | N/A | 0.48±0.00 | 2.2±0.1 | N/A | 0.31±0.02 |
| Aircraft, Southern Africa fresh[d] | N/A | 20±18 | 2±1 | N/A | 1.4±1.8 | 1.9±1.4 | 1.6±2.4 | 4.5±8.1 |
| Aircraft, Southern Africa aged[d] | N/A | 6±3 | 1.03±0.04 | N/A | 1.0±0.8 | 2.0±1.5 | 0.9±0.8 | 0.6±0.4 |
| Aircraft, Southern Africa, plume[e] | 106±86 | 91±74 | 15±12 | N/A | N/A | N/A | N/A | N/A |
| Aircraft, Southern Africa haze[e] | 10.5±8.2 | 9.5±6.8 | 2.3±1.8 | N/A | N/A | N/A | N/A | N/A |
| Aircraft, Southern Africa[f] | 8.5±4.8 | N/A | 2.3±1.9 | N/A | 0.8±0.3 | 4.5±3.6 | N/A | 0.4±0.1 |
| National Park, South Africa[g] | N/A | N/A | 1.2 - 2.2 | N/A | N/A | N/A | N/A | 0.22 - 0.34 |
| Savanna, South Africa[h] | 9.1 | N/A | 0.61 | N/A | 0.4 | 11.08 | 2.85 | 0.28 |
| Aircraft, W. Africa, bkg[i] | N/A | N/A | 0.33 – 0.35 | N/A | 0.11 – 0.12 | 1.64 – 1.70 | 0.63 – 0.68 | N/A |
| Aircraft, W. Africa, urban plume[i] | N/A | N/A | 0.64 – 0.72 | N/A | 0.49 – 0.53 | 2.70 – 3.03 | 1.20 – 1.38 | N/A |
| Grassland, South Africa, dry[j] | N/A | N/A | 0.6 | N/A | 0.3 | 1.4 | 0.2 | N/A |
| Grassland, South Africa, wet[j] | N/A | N/A | 0.3 | N/A | 0.2 | 0.4 | 0.3 | N/A |
| Savanna, South Africa, spring[k] | N/A | N/A | 0.40 | N/A | 0.05 | 2.48 | 0.05 | 0.17 |
| Savanna, South Africa, summer[k] | N/A | N/A | 0.16 | N/A | 0.01 | 5.65 | 0.01 | 0.2 |

a. Present study
b. Mkoma et al., 2014
c. Gao et al., 2003
d. Formenti et al., 2003
e. Kirchstetter et al, 2003
f. Sinha et al., 2003
g. Maenhaut et al., 1996
h. Puxbaum et al., 2000
i. Brito et al., 2018
j. Tiitta et al., 2014
k. Aurela et al., 2016

## FIGURES

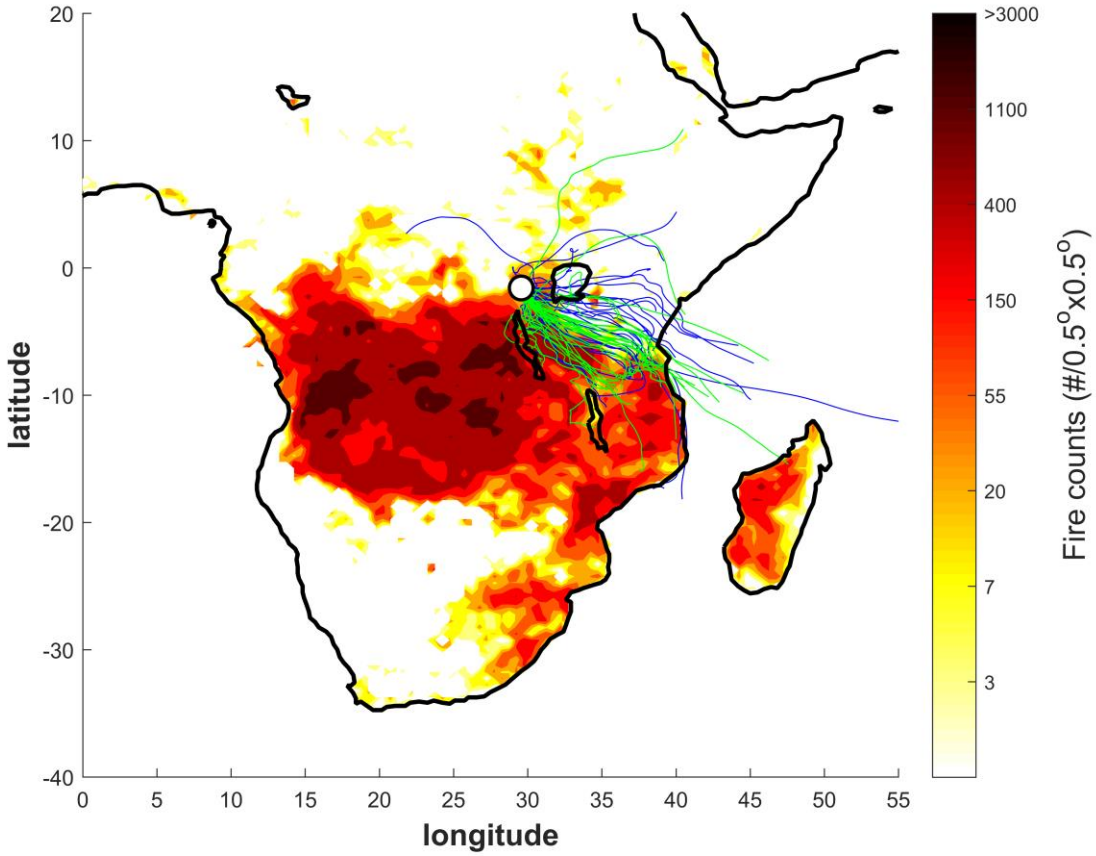


**Figure 1** Fire counts and air mass back trajectories for the October 2014 to September 2015 campaign at the Rwanda Climate Observatory (RCO, black and white circle). The fire counts are from the Fire Information for Resource Management System (FIRMS) derived from the NASA Moderate Resolution Imaging Spectroradiometer (MODIS) satellite product for June-July-August (JJA), 2015. The thin lines represent (4AM, C.A.T.) 5-day air mass back-trajectories arriving at RCO 100 m.a.g.l. (2690 m.a.s.l.). The blue lines correspond to what we here refer to as the 'wet' seasons (October-November 2014 and April-May 2015), whereas the green lines represent the dry JJA season.

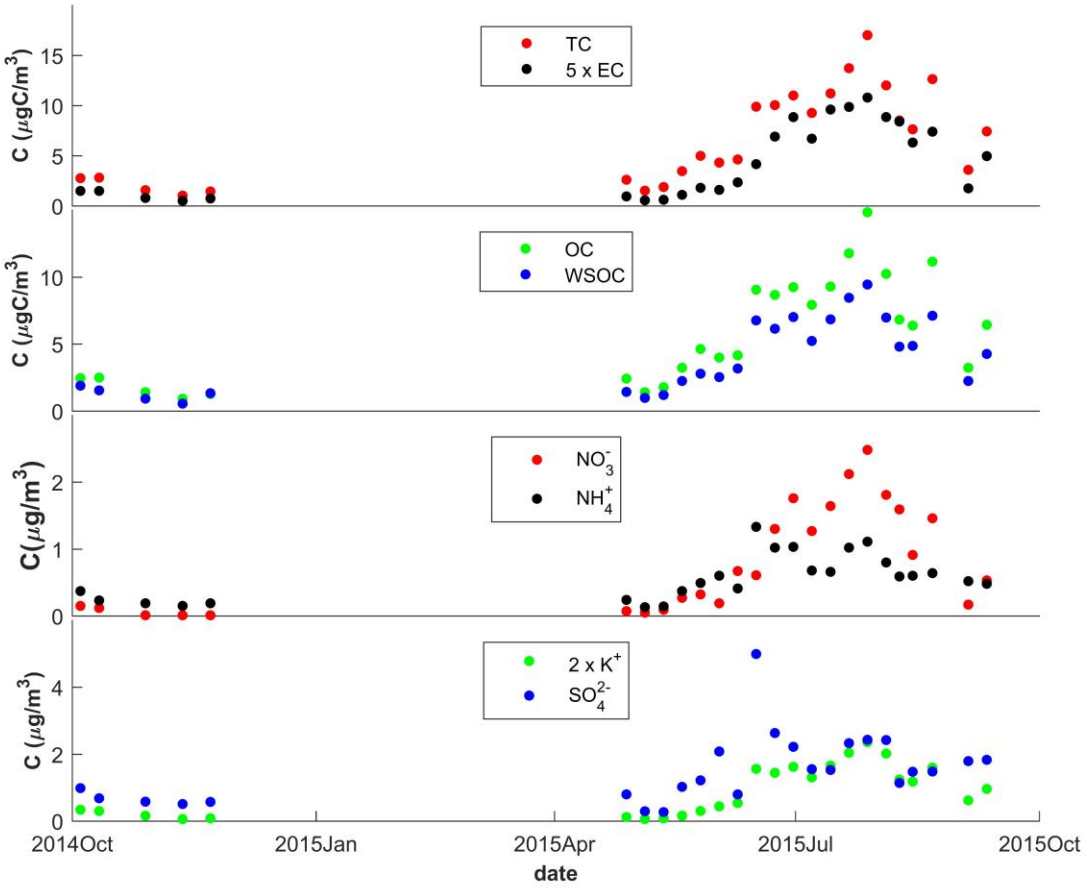


**Figure 2.** Concentrations of carbonaceous aerosols (TC = total carbon; EC = elemental carbon; OC = organic carbon; WSOC = water-soluble organic carbon) and inorganic ions in $PM_{2.5}$ during October 2014 to September 2015 at the Rwanda Climate Observatory. Instruments were hit by lightning resulting in a data gap November 2014 to April 2015. The concentrations of EC were multiplied by 5 and $K^+$ by 2 for visual clarity.

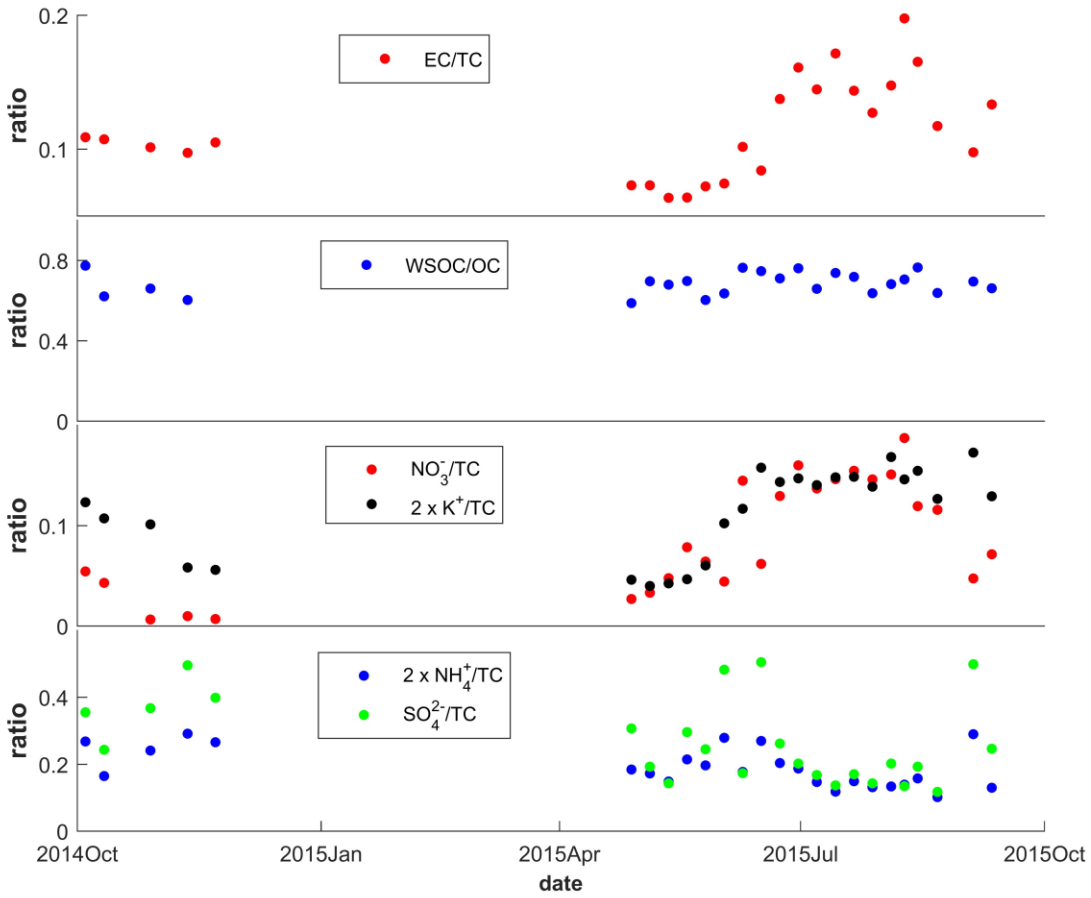


732

733 **Figure 3.** Ratios of carbonaceous aerosols (EC = elemental carbon; OC = organic carbon; WSOC
734 = water-soluble organic carbon) and inorganic ions relative to total carbon (TC) in $PM_{2.5}$ during
735 October 2014 to September 2015 at the Rwanda Climate Observatory. Instruments were hit by
736 lightning resulting in a data gap November 2014 to April 2015. The concentrations of $K^+$/TC and
737 $NH_4^+$/TC ratios were multiplied by 2 for visual clarity.

738

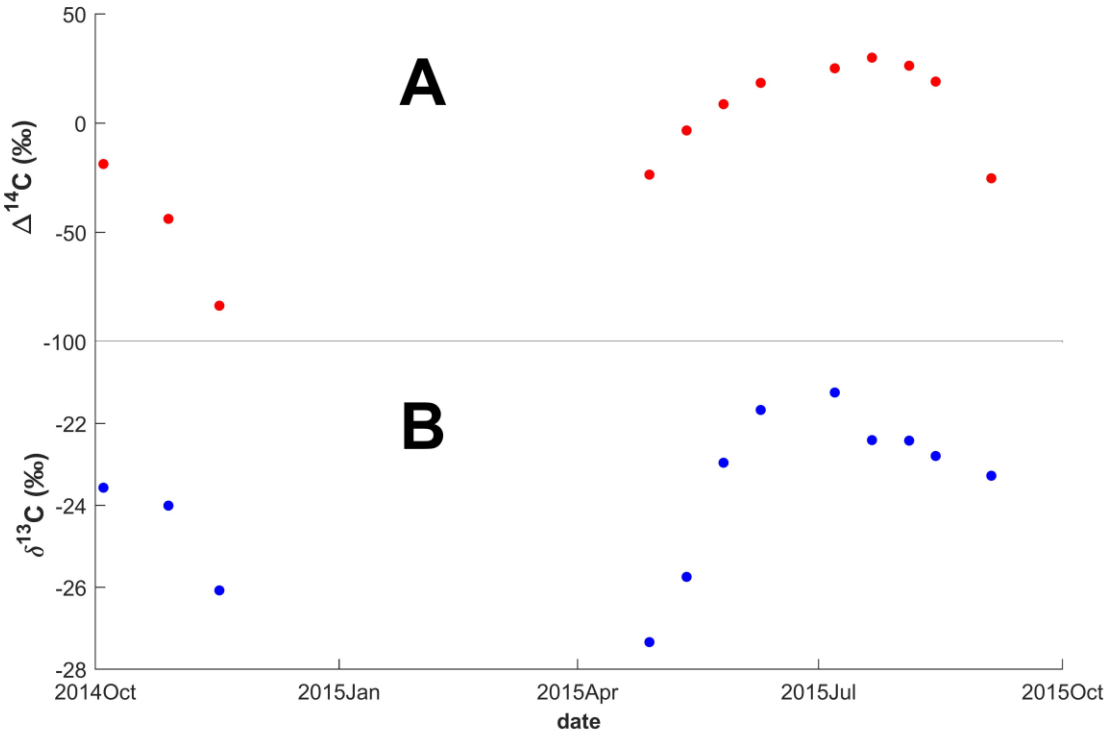


739

740 **Figure 4**: Dual carbon isotope data for TC vs time. Panel A. $\Delta^{14}C$ and Panel B. $\delta^{13}C$. The
741 uncertainties for $\Delta^{14}C$ are below 50‰ and ~ 0.2‰ for $\delta^{13}C$. Instruments were hit by lightning
742 resulting in a data gap November 2014 to April 2015.

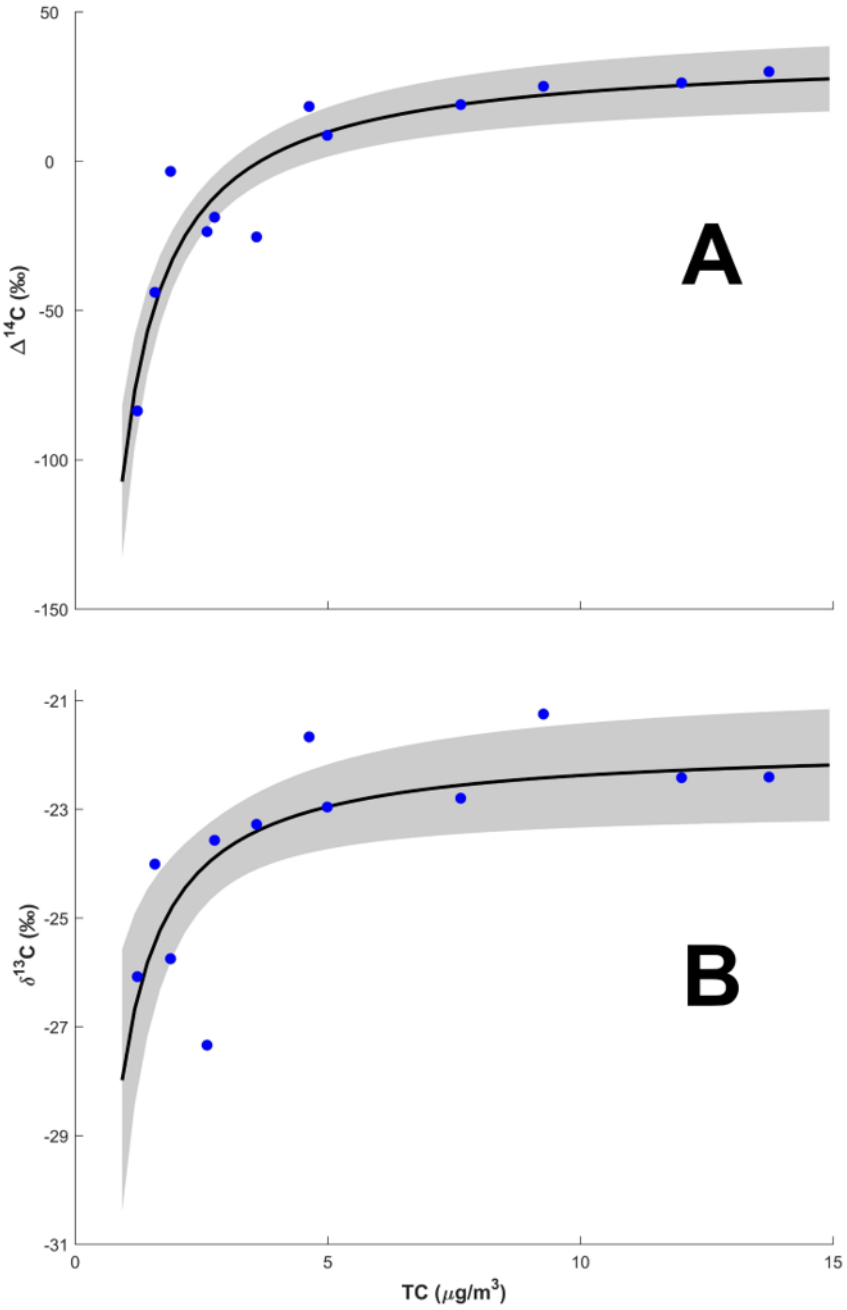


743

744 **Figure 5.** Interrelations of carbon isotope signatures and TC (blue circles). Panel A. $\Delta^{14}C$ vs TC,
745 Panel B. $\delta^{13}C$ vs TC. The black line is the mean fit of the equation $\Delta^{14}C$, $\delta^{13}C$ = A/[TC]+B, using
746 Markov chain Monte Carlo simulations, where A and B are fitting parameters. For $\Delta^{14}C$, A= -
747 135±16 ‰ µg $m^{-3}$; B= 37±6 ‰. For $\delta^{13}C$, A= -5.8±1.5 ‰; B= -21.8±0.6 ‰ µg $m^{-3}$. The grey
748 shaded area display the 1σ spread of the fit.

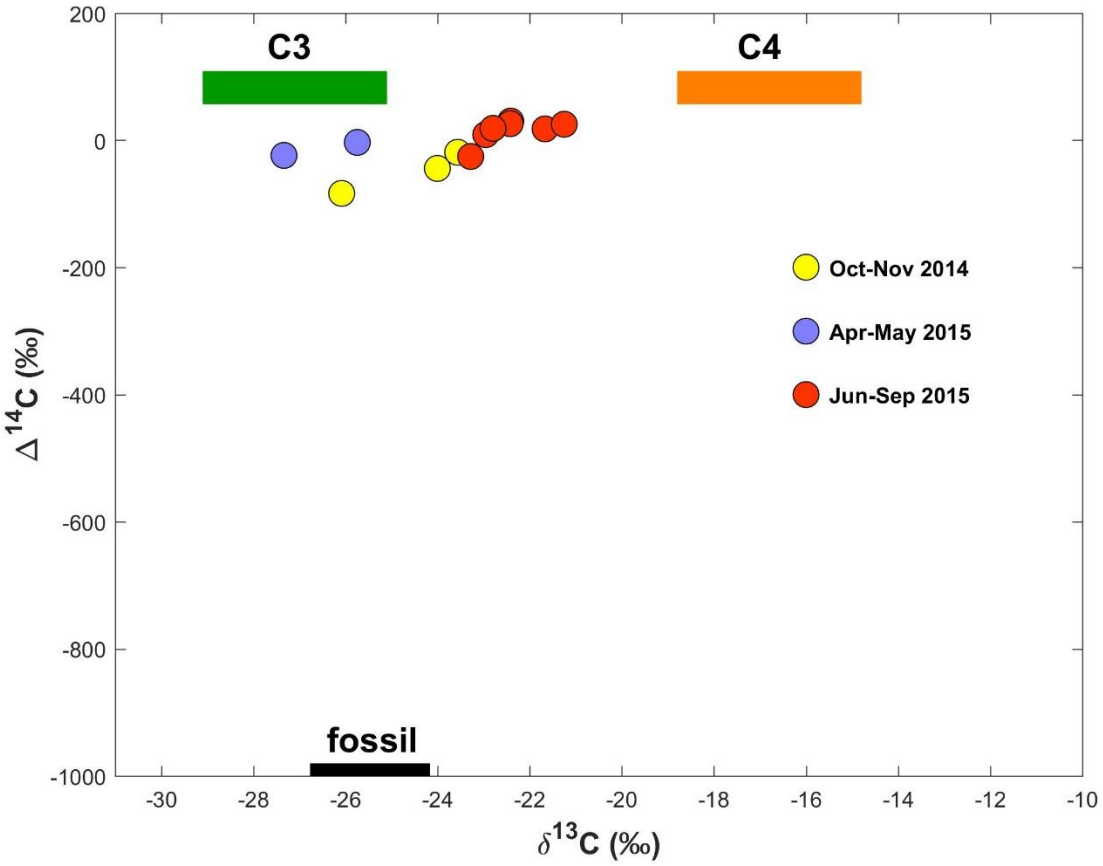


**Figure 6**: Dual carbon ($\Delta^{14}C$ vs $\delta^{13}C$) isotope plot of TC. Blue circles represent Oct-Nov 2014 (wet), yellow circles Apr-May 2015 (wet), and red circles Jun-Sept 2015 (dry). The boxes represent the endmember ranges (mean ± stdev; see Section 3.5 for details) of the three main sources: $C_3$-plants (green), $C_4$-plants (orange), and fossil (black).

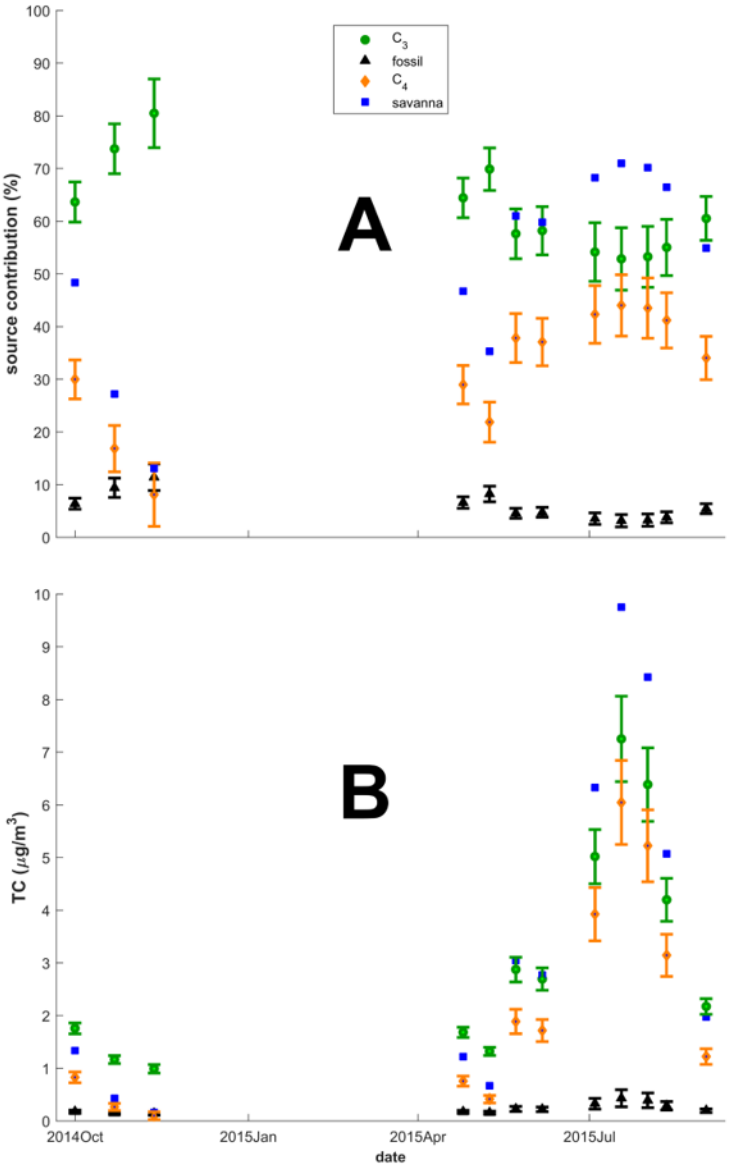


757

758 **Figure 7:** Carbon isotope source-segregated fractions and concentrations of TC vs time computed
759 with the 'best endmember scenario'. Panel A. Relative source contributions (%) of $C_3$-plants
760 (green circles), $C_4$-plants (orange diamonds) and fossil (black triangles). Estimated savanna
761 contributions are shown as blue squares. Panel B. Source segregated concentrations of TC of $C_3$-
762 plants (green circles), $C_4$-plants (orange diamonds) and fossil (black triangles). The error bars
763 (standard deviations) were calculated using Markov chain Monte Carlo simulations.

764